UNIVERSITÀ DEGLI STUDI DI NAPOLI
FEDERICO II

SCUOLA POLITECNICA E DELLE SCIENZE DI BASE

CORSO DI LAUREA IN INGEGNERIA AEROSPAZIALE

DIPARTIMENTO DI INGEGNERIA INDUSTRIALE

BACHELOR THESIS

PRELIMINARY SIZING, STABILITY, AND CONTROL OF AN ELECTRIC POWERED RC AIRCRAFT

SUPERVISOR:
Dr.
CILIBERTI DANILO

CANDIDATE:
FRANCESCO LOSAPPIO
Matricola: N35002452

CO-SUPERVISOR:
Prof. Eng.
NICOLOSI FABRIZIO

ANNO ACCADEMICO 2019/2020

AI MIEI GENITORI GIULIA E GIUSEPPE E AI MIEI

NONNI. UN PENSIERO SPECIALE A NONNO ALBERTO E

NONNO FRANCESCO

SIC PARVIS MAGNA

Index

List of figures

List of tables

Chapter 1
Introduction

1. Team Organization

The team appointed to the realization of the model is a subgroup of the team formed in 2019, to participate in the Design Build and Fly (DBF) competition, that would have been held the following year. The missions and requirements taken into consideration have been established starting from the ones of the competition. This project has given to each member of the team the opportunity to improve several soft skills, such as team working and problem solving, which are relevant and decisive for an engineer. In addition, this experience has allowed to deepen knowledge in the Aerospace Engineering field, providing the fundamentals of aircraft design in the context of an experimental bachelor's thesis.

The team counts five members to better focus each one's work on the five branches identified, that will lead to the final design of the aircraft, called by the team as "UninAir". Consequently, each member of the team is the leader of its own branch and therefore its manager. The team has been supervised by two advisors, who proved guidance to the team throughout the whole project. The identified branches concern: the study of the aerodynamics of the aircraft through the use of software such as AIRFOIL and XFLR5; examination of the stability of the model with the aid of the program created by NASA, OpenVSP; structural analysis, in particular an accurate check was performed on the wing structure, in presence of aerodynamic loads; aircraft performance analysis (polar curves, propeller performance). It is clear that each branch is not isolated from the others, but there is a strong link between all the application fields considered, therefore a coordinated work by each member of the Team is required.

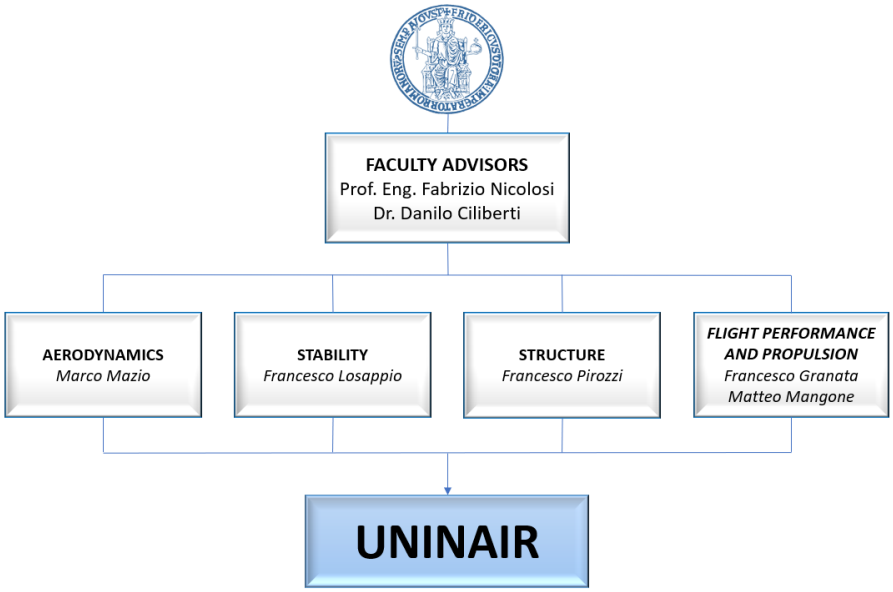

Figure 1 - Team Organization

1.1 Requirements

The main purpose of the team was to carry as many passengers as possible, in order to allow the aircraft to conduct charter flights recovering expenses. In the table below, there is an overview of the requirements that the team had to take into account during the project:

Table 1 – Requirements

Maximum allowable wingspan	$5\ ft = 1{,}5\ m$
Take-Off Gross Weight with payload	$TOGW < 55\ lb = 25\ kg$
Passenger Weight	$5\ oz = 113{,}4\ g$
Luggage Weight	$1\ oz = 28{,}35\ g$
Take-Off Run	$23\ ft = 7\ m$
Ground for the take-off	$Dirt$
Endurance	$10\ min$
Minimum load for bending test	$\pm\ 3x\ MTOW$
Type of Propulsion	$Electric$

In addition, the aircraft has to follow the path shown in the figure, and each lap must be completed in 2 minutes, in order for passengers to have a comfortable and safe flight.

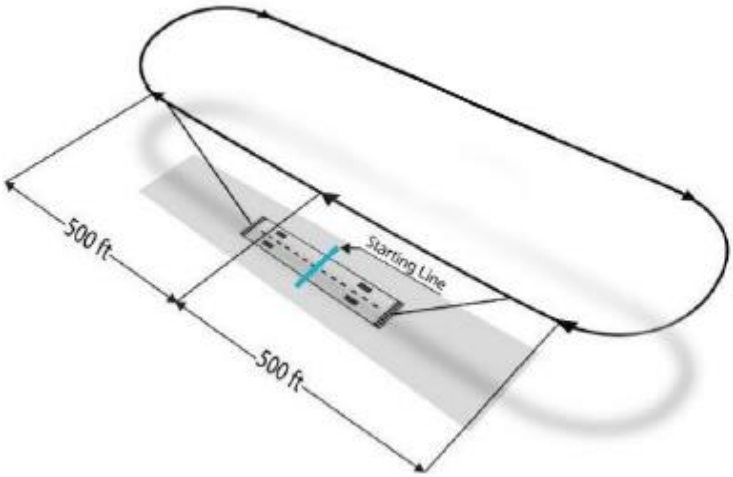

Figure 2 - AIAA Competition Flight Course

The dimension of each passenger and luggage are defined in the figures below:

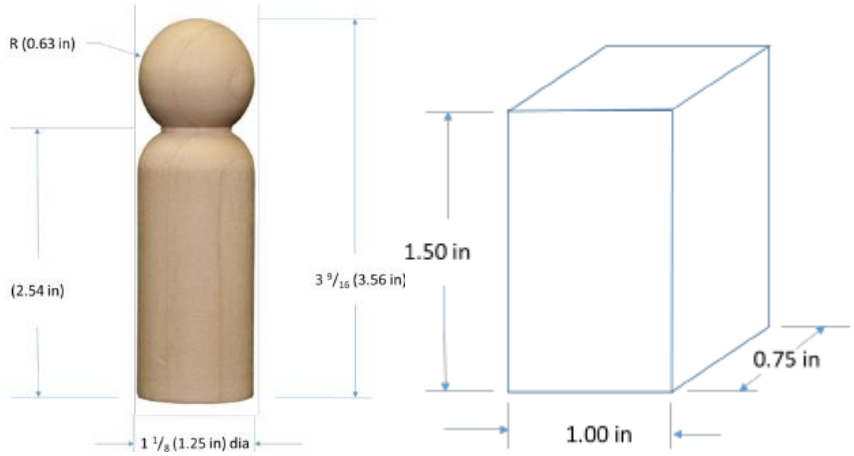

Figure 3 - Passenger and Luggage

Chapter 2
Preliminary Design and Sizing

2. Design Selection Process

In order to properly choose the best configuration for the aircraft, the team has compiled a table of merit, based on the most important configuration factors. It has been assigned a score from 0 to 5 for each one, depending on the mission requirements.

Table 2 - Table of merit

Factor	Importance
Structural Weight	4
Maneuverability	3
Passengers Capability	5
Speed	3,5
Manufacturability	4,5
Take-OFF Run	2,5
Reliability	2,5

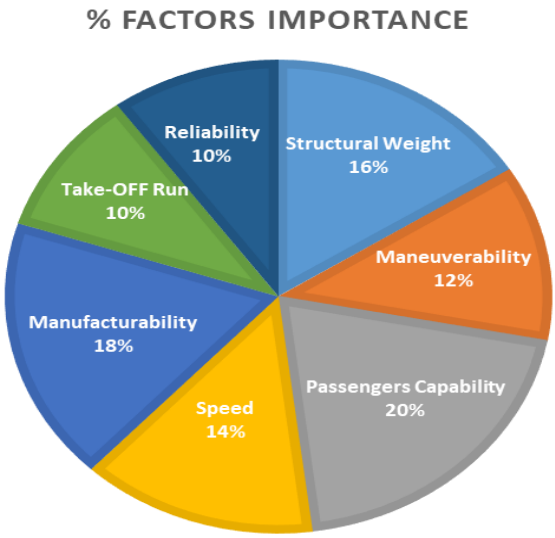

- **Structural Weight**: the weight strongly influences the performance of the aircraft, indeed a lower structural weight means either less consumption or more payload transportable.
- **Maneuverability**: the capability to safely control the aircraft, its stability, as well as fast maneuvers, are also important to complete all the laps on time.
- **Passengers Capability**: this is the most important factor, because carrying as many passengers as possible would provide more income for the charter company.
- **Speed**: the airplane speed contributes to complete faster the mission, although a trade-off study is necessary to avoid an excessive consumption of the batteries.

- **Manufacturability**: the ease of manufacturing is essential to build the aircraft by the team itself. Therefore, some configurations have been rejected due to tricky manufacturing and lack of solid executive experience alike.
- **Take-Off Run**: having a short take-off run is part of the requirements. This aspect forced the team to take into account configurations that would provide advantages on those terms.
- **Reliability**: to guarantee the safety during the missions (take-off, cruise and landing), the reliablitiy of the aircraft is not a negligible factor.

Table 3 - Final Design Decision

Feature	Configuration	Wing	Tailplane	Engine	Landing Gear	Fuselage
Result	CONVENTIONAL	LOW	CONVENTIONAL	SINGLE/TWIN	TRICYCLE	RECTANGULAR

The final conceptual design has been chosen by analyzing the total score gained by each different configuration, in terms of Structural Weight, Maneuverability, Passenger Capability, Speed, Manufacturability, Take-off Run and Reliability as shown so far. The total score is obtained by adding up scores assigned to each possible configuration, as it will be shown further into the study.

2.1 Conceptual Design

Considering the requirements of the mission, it is appropriate to present the layout of the team's arguments, regarding how the bulk of the design was figured out. As a general note, the focus was on:

- Main wing configuration
- Main wing positioning
- Tail section
- Engines
- Landing gear
- Fuselage

This preliminary discussion has been crucial in order to further analyse the capabilities of the aircraft. The following choices formed the foundations of the specialized studies, whose aim is to reach the optimal configuration.

Table 4 - Design Alternatives

Component	Alternatives		
Wing Layout	Conventional	Biplane	Flying Wing
Wing Positioning	Low	High	
Empennage Type	V-Tail	Conventional	T-Tail
Number of Engines	1	2	
Landing Gear	Taildragger	Tricycle	
Fuselage section	Smoothed Rectangular	Circular	

2.1.1 Main Wing Configuration

The choice of the main wing configuration of the aircraft is the first aspect that was taken into account. That is because it is important to adapt the subsequent decisions regarding the individual components of the aircraft to this primary one.

The considered configurations are:

- CONVENTIONAL: it is composed by the tail plane (horizontal and vertical) and one main wing.
- BIPLANE: two overlapping wings which are parallel to each other although they may have different shapes and sizes.
- FLYING WING: flying wing aircraft without fuselage and tail plane.

By a structural weight's point of view, the best one is the flying wing since it is the lightest, because of the tail plane absence. However, the flying wing does not excel on directional stability, due to the absence of the fin and this directly affects manoeuvrability. It is important to point out that the flying wing configuration will have a high longitudinal stability, if equipped with reflex airfoil (self-stable) and if the warping factors and the sweep angle are well evaluated.

Regarding the biplane it is important to note that with the same wingspan of a conventional configuration, there is twice as much wing area, halving the wing load. Moreover, the eventual presence of a double aileron implies a higher roll rate, and therefore more lateral manoeuvrability.

Focusing on reliability, the conventional configuration is the best known of the three considered, therefore well proven to be dependable. The biplane is frequently subject to assembly inaccuracies since it is the most complex.

Both the biplane and flying wing models are very difficult to manufacture, because they require unconventional construction techniques. On the other hand, the conventional configuration is the simplest to manufacture.

The flying wing is the one that generates less drag among the three. On the other hand, the biplane configuration, with the presence of two main lift generators, create four vortex that massively increases aerodynamic drag. The conventional one is a good compromise between the previous two.

Regarding the passenger's capacity, the biplane is the most inconvenient because it is difficult to create a passage for the insertion of passengers, due to the presence of wing braces between the two wings.

Biplane configuration has a lower take off length since, with the same wingspan, the wing surface is two times bigger and therefore the wing load decreases. The opposite situation occurs with the flying wing, also because of the lack of flaps.

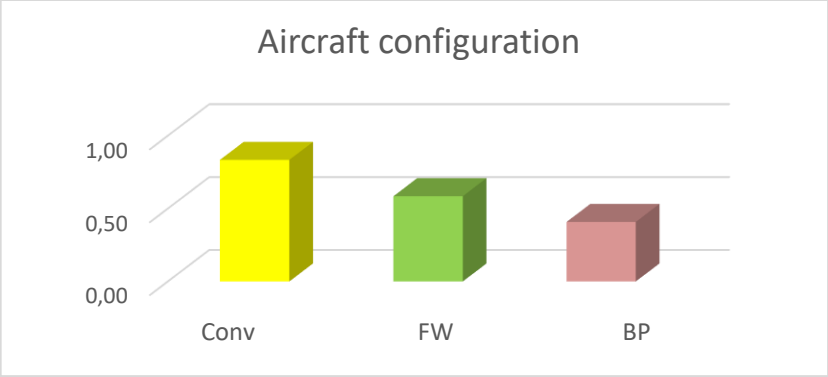

Figure 4 - Configuration Trade Study

Table 5 - Configuration Trade Study

CONFIGURATION TRADE STUDY							
		CONVENTIONAL		FLYING WING		BIPLANE	
Attribute	Weighting	Insert Score	Weighted score	Insert Score	Weighted score	Insert Score	Weighted score
Structural Weight	16%	0.6	0.096	1	0.16	0.3	0.048
Manoeuvrability	12%	0.8	0.096	0.5	0.06	0.6	0.039
Passengers Capability	20%	0.8	0.16	0.3	0.06	0.7	0.081
Speed	14%	0.8	0.112	1	0.14	0.4	0.037
Manufacturability	18%	1	0.18	0.25	0.045	0.5	0.065
Take-Off Run	10%	0.9	0.09	0.7	0.07	1	0.083
Reliability	10%	1	0.1	0.5	0.05	0.6	0.055
Totals	100%		0.83		0.59		0.41

2.1.2 Wing Positioning

Once opted for the conventional configuration for our aircraft, two different wing positions have been taken into consideration: high wing and low wing. As it is showed in the table below, the passenger capability is the parameter which most influenced the choice.

In terms of structural weight, the low wing configuration is slightly better, because it allows to embed the spar in the force frames. This is not possible with a high wing that should be installed on the upper surface of the fuselage. However, in case of braced wing, the root sections could be slenderer because in that zone the momentum is null.

An aircraft with high wing has a better (static) lateral stability thanks to the dihedral effect (which gives a negative injection to the coefficient $C_{\mathcal{L}_\beta}$). Indeed, as shown in the figure below, a side wind (i.e. sideslip) causes an overpressure under the upwind wing and therefore the aircraft tends to stabilize thanks to the rolling moment generated. On the other hand, low wings provide better aerodynamic performance, due to the absence of the joints between wing

and fuselage, that is less interference drag. Moreover, it might help to reduce the take-off run taking advantage of the ground effect.

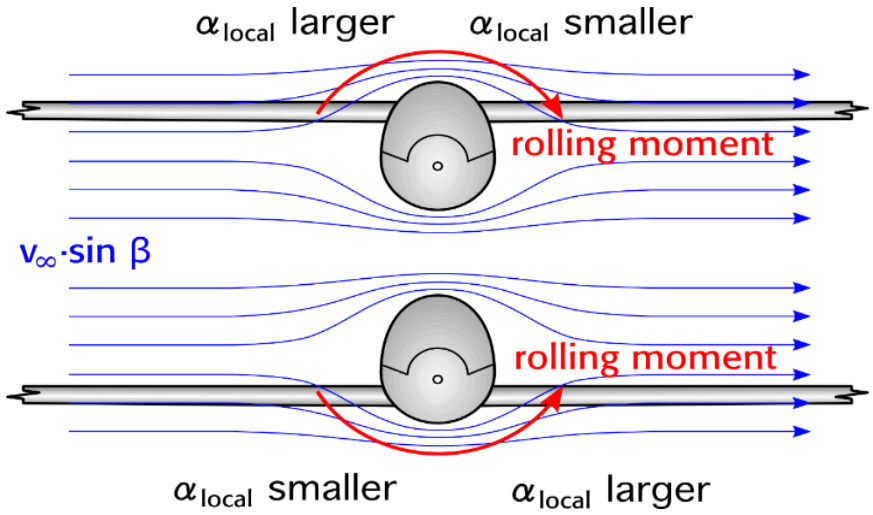

Figure 5 - Rolling Moment

As regards reliability, in case of imprecise landing, the high wing configuration is safer because the clearance is greater than it is with the low wing one which, instead, may impact on the ground if the airplane is banked.

The most important feature of the low wing configuration is that it guarantees a straightforward building and a simple access to the compartment, where the passengers and luggage are stored. In addition, this configuration makes the assembly of the wing easier or its substitution alike. On the contrary, with a high wing, the loading and unloading of payload is likely to be trickier.

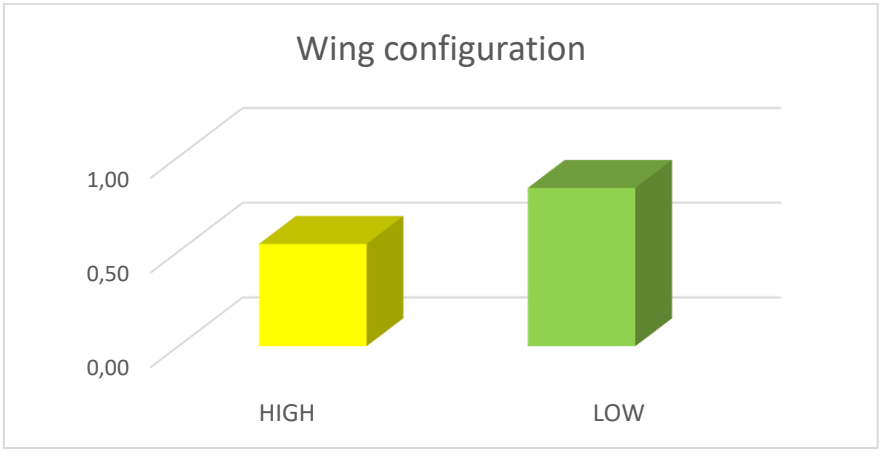

Figure 6 - Wing Configuration Trade Study

Table 6 - Wing Configuration Trade Study

WING CONFIGURATION TRADE STUDY					
		HIGH		LOW	
Attribute	Weighting	Insert Score	Weighted score	Insert Score	Weighted score
Structural Weight	16%	0.4	0.064	1	0.16
Manoeuvrability	12%	0.6	0.072	0.8	0.096
Passengers Capability	20%	0.5	0.1	1	0.2
Speed	14%	0.4	0.056	0.7	0.098
Manufacturability	18%	0.6	0.108	0.9	0.162
Take-Off Run	10%	0.5	0.05	0.8	0.08
Reliability	10%	0.9	0.09	0.4	0.04
Totals	100%		0.54		0.836

2.1.3 Tail

Once the configuration of the main wing is established, it is fundamental to discuss characteristics of the tail plane, specifically on a matter of stability, controllability, and reliability.

The main types of tail planes currently adopted by the aerospace industry are: conventional, T-tails, and V-tails. All of those options provide the aircraft with specific advantages and drawbacks that require a careful analysis.

It seems clear that the weight of the structure that support the aerodynamic surfaces of the tail plane will not be a major point of this discussion since it contributes only by a little percentage (estimated 5%) of the total inertial forces of the model aircraft.

The key point to analyse is instead how a different configuration plays into the overall stability and control of the aircraft, underlining the effect that each one has on the take-off distance.

The T-tail is composed by a vertical stabilizer which holds, within itself, the support structure of the horizontal stabilizer, placed at its tip. This particular kind of tail plane offers the advantage of working in an undisturbed airflow, allowing it to generate more lift at lower speed. Indeed, the dynamic pressure hitting the horizontal plane is unaffected by the downwash of the main wing, bringing the $\eta_H \cong 1$. At the same time, the horizontal tail reduces the magnitude of the vertical tail tip vortex, increasing the vertical tail effectiveness in sideslip, a phenomenon called end-plate effect.

Many times these advantages are outshined by a safety flaw of the T configuration. On extreme stall condition, the cone of turbulent flow coming from the main wing might engulf the tail plane, reducing its power of control turning it not effective altogether. This reason, along with an increased load on the vertical stabilizer, brought the team to reject the T-tail configuration.

T-tail is also prone to flutter, a dynamic aeroelastic phenomenon that must be avoided to fly safely. Tail flutter can rapidly destroy the empennage, leaving the aircraft without stability and control. To avoid flutter, the T-tail must have a very strong and rigid structure, which will increase the structural weight, opposing its aerodynamic advantage.

In contrast with all standard configurations, the V-tail consists in only two aerodynamic surfaces, they are tilted at an angle and often fixed on the upper side of the aircraft, effectively getting rid of one of the three wings that form the usual tail plane design. This of course makes the tail lighter, but, as we previously discussed, that is not an important issue for the analysis. Once again, the focus is on the ability of this configuration to provide stability and control authority during flight. The main feature of the V-tail is that the control power of rudder and equalizer is mixed and enforced using only two control surfaces. Yaw and pitch are consequently less effective unless the dimensions of the tail increase. This potential lack of power of the mixed equalizer might also result into a less performant take-off, that is one of the given requirements for the aircraft.

Therefore, the attention was focused on the conventional design for the tail plane. Both the deeper understanding for its properties and the possibility of installing a stabilator (since the stabilator is fitted into the fuselage) give this design an edge over the other two.

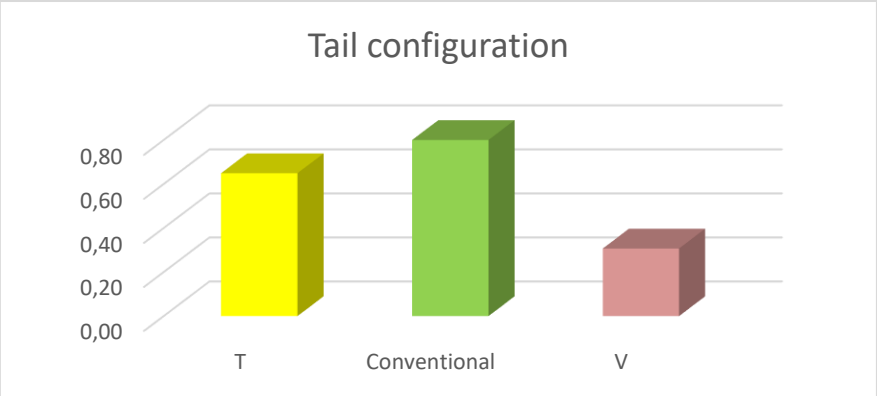

Figure 7 - Tail Configuration Trade Study

Table 7 - Tail Configuration Trade Study

TAIL CONFIGURATION TRADE STUDY							
		T		Conventional		V	
Attribute	Weighting	Insert Score	Weighted score	Insert Score	Weighted score	Insert Score	Weighted score
Structural Weight	16%	0.7	0.112	1	0.16	0.5	0.08
Manoeuvrability	12%	1	0.120	1	0.120	0.2	0.024
Passengers Capability	20%	0	0.000	0	0.000	0	0.000
Speed	14%	0.8	0.112	1	0.140	1	0.140
Manufacturability	18%	0.75	0.135	1	0.180	0.1	0.018
Take-Off Run	10%	1	0.100	1	0.100	0.25	0.025
Reliability	10%	0.7	0.070	1	0.100	0.2	0.020
Totals	100%		0.65		0.80		0.31

2.1.4 Number of Engines

Several factors were taken into account while conducting the propulsion system trade study for the aircraft. In particular, the aim of this section is to understand what the best number of

engines is to install on the aircraft and therefore choose the single-engine configuration or the twin-engine configuration.

Firstly, a single engine configuration shall guarantee a certain overall weight saving since the battery pack should be lighter than the one needed for two engines. On the other hand, while a single engine would be installed on the aircraft's nose, in case of the twin-engine configuration, the engines would be installed on the wing structure. The presence of two inertial masses on the wing would make the total wing load decrease, thus the wing itself would be less stressed during flight. However, if the engines are installed on the wing, then a strengthened structure is needed where the engines are attached to the wing. That might mitigate the weight advantages aforementioned and would undermine the ease of manufacturing of the wing. Moreover, the CG of the wing sections that are behind the engine might shift ahead of the aerodynamic centre. This might increase the torque insisting on the wing structure.

The position of the engines also influences the manoeuvrability and stability of the aircraft. If the engine is on the aircraft's nose then it will not be influenced by the upwash generated by the wing, therefore the phenomena of non-axial flow, derived by the interaction air-wing, can be ignored. Furthermore, the energised flow behind the propeller increases the efficiency of the aerodynamic surfaces both of the horizontal tail plane and, in a lesser extent, the main wing. However, a twin-engine configuration ensures a better lateral control as it is possible to realise a differential thrust in order to help the rudder in case of need. At the same time, two engines require a bigger and strengthened rudder because it must guarantee directional controllability in case of one inoperative engine (OEI). It has to be said that in the unlucky event of a double engine failure, the presence of two propellers would induce more drag on the gliding aircraft than it would be if there was only one engine.

Moreover, two engines installed on the wing might be an obstacle while loading and unloading passengers as they would be close to the fuselage part that needs to be open during ground operations. Thus, for this reason and to guarantee a certain clearance from the ground, the propellers' diameter might need to be too limited. While it is true that in case of OEI condition a twin-engine configuration doesn't force the aircraft to abort the mission it is meant to accomplish, it also requires a more complicated electrical system and one more channel on the aircraft's controller than the single-engine configuration. Two engines also imply more maintenance and greater difficulty in case of substitution or repair of one of the engines.

In fact, it is not possible to decide without more specific considerations which configuration to choose. Therefore, once the aircraft geometry and structural characteristics will be more or less fixed, both studies about the single-engine and the twin-engine configuration will be further conducted to have a better understanding of the problem.

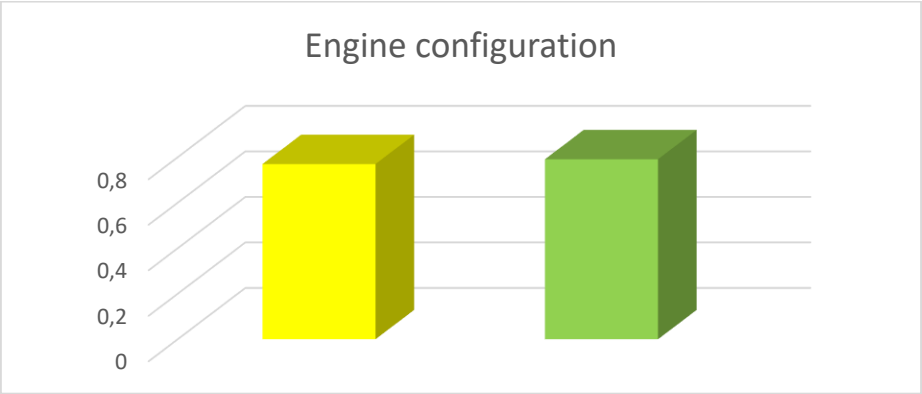

Figure 8 - Engine Configuration Trade Study

Table 8 - Engine Configuration Trade Study

ENGINE CONFIGURATION TRADE STUDY					
	N	single		twin	
Attribute	Weighting	Insert Score	Weighted score	Insert Score	Weighted score
Structural Weight	16%	1	0.16	0.5	0.08
Manoeuvrability	12%	1	0.120	0.3	0.036
Passengers Capability	20%	0.6	0.120	1	0.200
Speed	14%	0.5	0.070	1	0.140
Manufacturability	18%	1	0.180	0.75	0.135
Take-Off Run	10%	0.7	0.070	1	0.100
Reliability	10%	0.5	0.050	1	0.100
Totals	100%		0.77		0.79

2.1.5 Landing Gear Type

Two different types of landing gear were compared. The first one is the tricycle landing gear that has a single nose wheel in the front, and two main wheels positioned close to the centre of gravity. The other alternative is the bicycle landing gear, also known as “taildragger”, which consists in a pair of wheels ahead the centre of gravity with an additional smaller wheel in the back of the plane.

By comparing the two solutions it was deduced that the tricycle leads to a greater structural weight than the bicycle. However, the weight gap is not wide enough to consider this aspect as a key factor for choosing one upon the other.

From the manoeuvrability point of view, it was found that the tailwheel-type landing gear, forces the aircraft to have a lower pitch angle during landing. That implies a strong use of the elevators to ensure a correct manoeuvre. Moreover, the relative position of CG and main landing gear does not mitigate the effect of the momentum generated by the friction between wheels and runway. Therefore, the rudder needs to make the aircraft stable also once it has touched the ground. On the other hand, the tricycle landing gear lets the aircraft fly at a greater angle of attack during approach to the runway, reducing landing speed and making the landing manoeuvre safer. The tricycle is also more stable during landing especially in case of single-engine configuration, as it guarantees more support to nose’s structure that carries the propeller and the engine.

The two-wheeled gear is aerodynamically convenient because the area exposed to the airflow is less than it is in the tricycle configuration.

The final boardable number of passengers will not be significantly affected by one of the different configurations considered. However, the tricycle is more comfortable because it does not involve any inclination of the fuselage during ground operations, so it is easier to load/unload passengers.

In case of the bicycle landing gear there is a greater inclination between the aircraft and the ground which implies a drag increment and it complicates the take-off manoeuvre. This condition stands until the aircraft is aligned with the runway. The bicycle landing gear is also preferable on grass airfield. On the other hand, the tricycle landing gear gives some advantages in terms of thrust during the take-off run because the thrust vector is parallel to the ground.

That allows a greater acceleration to quickly reach lift-off speed. This alternative is most suitable for asphalted runways.

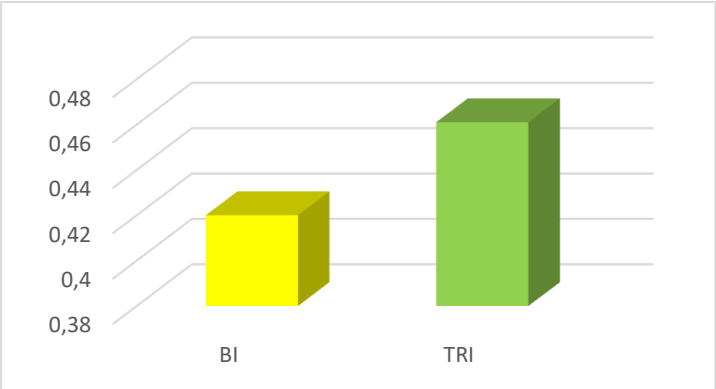

Figure 9 - Landing Gear Configuration Trade Study

Table 9 - Landing Gear Configuration Trade Study

GEAR CONFIGURATION TRADE STUDY					
		BI		TRI	
Attribute	Weighting	Insert Score	Weighted score	Insert Score	Weighted score
Structural Weight	16%	1	0.16	0.8	0.128
Manoeuvrability	12%	0	0.000	0	0.000
Passengers Capability	20%	0	0.000	0	0.000
Speed	14%	1	0.140	0.95	0.133
Manufacturability	18%	0	0.000	0	0.000
Take-Off Run	10%	0.7	0.070	1	0.100
Reliability	10%	0.5	0.050	1	0.100
Totals	100%		0.42		0.46

2.1.6 Fuselage

The key factor for the analysis of the fuselage is the amount of payload it can carry. The types of fuselage taken into account are:

- CLASSIC: lobe structure which allows to define a practical shell structure involving curved plated beams and fuselage former.
- SMOOTHED RECTANGULAR: rectangular structure characterised by several corners that allow the structure itself to absorb greater loads. This phenomenon, however, means that in those points there is a greater probability of cracks propagation.

The smoothed rectangular section has a greater ease of construction and a better exploitability (more usable volume for a given section area) than the circular section.

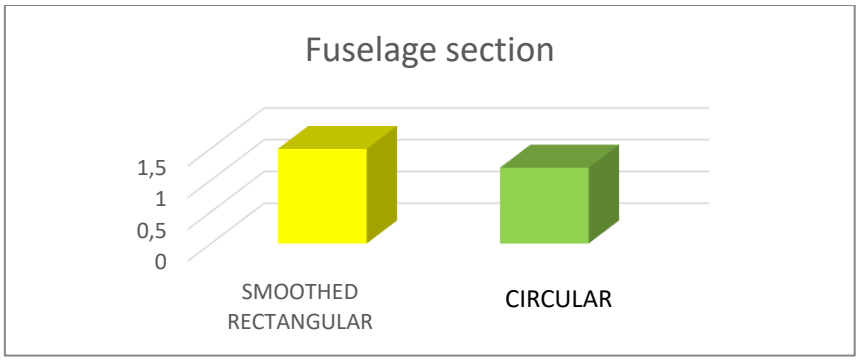

Figure 10 - Fuselage Configuration Trade Study

Table 10 - Fuselage Configuration Trade Study

FUSELAGE SECTION CONFIGURATION TRADE STUDY					
		SMOOTHED RECTANGULAR		CIRCULAR	
Attribute	Weighting	Insert Score	Weighted score	Insert Score	Weighted score
Structural Weight	16%	1	0.16	1	0.16
Manoeuvrability	12%	0	0.000	0	0.000
Passengers Capability	20%	1	0.200	0.75	0.150
Speed	14%	0.75	0.105	1	0.140
Manufacturability	18%	1	0.180	0.4	0.072
Take-Off Run	10%	0	0.000	0	0.000
Reliability	10%	1	0.100	0.75	0.075
Totals	100%		0.745		0.597

2.2 Sizing Process

Estimating dimensions and weights of the aircraft is a crucial phase of the design process and it allows the team to develop more detailed analysis based on aerodynamics, structures, and flight performance. The sizing process consists in an iterative procedure which starts giving as input the wing load *W/S* (statistically set), a plausible take-off and landing lift coefficient and the distance of the take-off run according to the requirements. The process ends when the variation of the final weight assumes a value within the 3% compared to the previous iteration.

Before calculating the weights, the determination of the power loading $\frac{W}{\Pi}$, where W is the max take-off weight and Π is the engine max power, is essential. First of all, the stall speeds during landing and take-off are easily calculable knowing the density of the air, the wing load, and the two lift coefficients $C_{L_{max_L}}$ and $C_{L_{max_{TO}}}$.

After that, according to the constraint about the take-off distance, it is possible to establish the thrust-to-weight ratio by using the simplified formula of the take-off run as it follows:

$$S_G = \frac{1.21\ W/S}{\rho g C_{L_{max_{TO}}}\ T/W} \quad \rightarrow \quad \frac{T}{W} = \frac{1.21\ W/S}{\rho g C_{L_{max_{TO}}} S_G}$$

Since the aircraft is propeller-driven, the power instead of the thrust has been considered during calculations. A proper approximation in take-off conditions is:

$$T = \frac{\Pi \eta_p}{0.7 \cdot 1.21 V_{S_{TO}}}$$

Furthermore, assuming a propeller efficiency η_p value relatively low (between 0.5 and 0.6), the following relation has been considered:

$$\frac{\Pi}{W} = \frac{0.7 \cdot 1.21^2\ W/S\ V_{S_{TO}}}{\eta_p \rho g C_{L_{max_{TO}}} S_G}$$

2.2.1 Weight Estimation

The characteristic weights of the aircraft are estimated in the following way.

The total weight (W) is given by the sum of different parts: structure, payload, engine (including prop), batteries, electronic parts. Passengers and their luggage constitute the payload to carry. They are respectively represented by standard cylinders and parallelepipeds made of wood. Their single weight is established by the requirements.

$$W = W_{\text{struct}} + W_{\text{payload}} + W_{\text{engine}} + W_{\text{batteries}} + W_{\text{electronic pts.}}$$

The structure's weight can be expressed by the following relation which takes into account the weight of the different structural components:

$$W_{\text{struct}} = W_{\text{wing}} + W_{\text{fuselage}} + W_{\text{h-tail}} + W_{\text{v-tail}} + W_{\text{gear}}$$

It is possible to statistically determine these weights by considering other aircraft with similar manufacturing characteristics (i.e. aircraft made of balsa wood). Then it is possible to evaluate for each component the weight to area ratio $W_{\text{comp}}/S_{\text{ref}}$ where S_{ref} is a characteristic surface of the component itself. That surface will be represented by the planform area for the wing and by the product of diameter and length for the fuselage (or eventually only for the length of the

part with a constant cross section). The landing gear data can be obtained from statistics or relating it to the total weight. The $S_{\text{h-tail}}$ is considered as the 20-30% of the S_{wing}

$$\frac{W_{\text{wing}}}{S_{\text{wing}}} \quad \frac{W_{\text{fuselage}}}{D_{\text{fuselage}} L_{\text{fuselage}}} \quad \frac{W_{\text{h-tail}}}{S_{\text{h-tail}}} \quad \frac{W_{\text{v-tail}}}{S_{\text{v-tail}}} \quad \frac{W_{\text{gear}}}{S_{\text{gear}}} \quad \left(\text{or } \frac{W_{\text{gear}}}{W}\right)$$

The structure weight relation can be then developed by using these ratios as it follows:

$$W_{\text{struct}} = \frac{W_{\text{wing}}}{S_{\text{wing}}} S_{\text{wing}} + \frac{W_{\text{fuselage}}}{S_{\text{fuselage}}} S_{\text{fuselage}} + \frac{W_{\text{h-tail}}}{S_{\text{h-tail}}} S_{\text{h-tail}} + \frac{W_{\text{v-tail}}}{S_{\text{v-tail}}} S_{\text{v-tail}} + \frac{W_{\text{gear}}}{S_{\text{gear}}} S_{\text{gear}}$$

An iterative process is necessary as the surfaces considered before are initially unknown. Firstly, the areas values are assumed, then the weights of the single components are estimated as well as the total weight. Thus, the wing surface and the engine's weight can be determined by using the wing load and the power load previously obtained. The process explained is repeated until the difference between two consecutive iterations is less than 10 g.

It is assumed a wingspan of 5 ft by referring to the constraints given by the requirements and a value for the aspect ratio (i.e. AR = 8). It is also considered a rectangular wing because of its ease of manufacturing and its cost benefits:

$$AR = \frac{b^2}{S} \quad S = \frac{b^2}{AR}$$

$$S = bc \quad c = \frac{S}{b}$$

At this point it is necessary to check whether the chord's length obtained is realistic comparing it to the fuselage one. While length and diameter of the fuselage depend on the payload, the tail and nose lengths are statistically determined by considering the ones of similar aircraft.

As the structure weight is now known, the weight of electronic parts, engines and batteries needs to be defined. This is possible by using catalogues on the internet which associates the maximum power supplied by the engine to its weight and to recommended electronic parts, such as ESC and batteries. The following ratios can be then determined assuming an initial power of 300-600 W:

$$\frac{W_{engine}}{\Pi} \quad \frac{W_{\text{batteries}}}{\Pi} \quad \frac{W_{\text{electronic pts.}}}{\Pi}$$

Table 11 – Iterations

ITERATIONS									
		ITERATION N. 1		ITERATION N.2		ITERATION N.3		ITERATION N.4	
Name	**Symbol**	**Quantity**	**Unit**	**Quantity**	**Unit**	**Quantity**	**Unit**	**Quantity**	**Unit**
Power needed	Π_n	150.77	W	152.46	W	152.92	W	153.04	W
ENGINE SYSTEM WEIGHT CALCULATION									
Engine weight	W_{engine}	0.044	Kg	0.045	Kg	0.045	Kg	0.045	Kg
Battery weight	$W_{battery}$	0.108	Kg	0.109	Kg	0.109	Kg	0.109	Kg
ESC weight	W_{ESC}	0.016	Kg	0.016	Kg	0.016	Kg	0.016	Kg
Engine Syst. weight	$W_{engine.pts.}$	0.168	Kg	0.170	Kg	0.171	Kg	0.171	Kg
STRUCTURAL WEIGHT CALCULATION									
Wing surface	S_{wing}	0.292	m^2	0.296	m^2	0.296	m^2	0.297	m^2
Fuselage diameter	D_{fus}	0.130	m	0.130	m	0.130	m	0.130	m
Fuselage length	L_{fus}	0.738	m	0.738	m	0.738	m	0.738	m
Horizontal tail surface	S_{H_tail}	0.058	m^2	0.059	m^2	0.059	m^2	0.059	m^2
Vertical tail surface	S_{V_tail}	0.020	m^2	0.021	m^2	0.021	m^2	0.021	m^2
Structural weight estimate	W_{struct}	1.417	Kg	1.424	Kg	1.426	Kg	1.426	Kg
Payload weight	$W_{payload}$	1.371	Kg	1.371	Kg	1.371	Kg	1.371	Kg
Total aircraft weight	W_{tot}	2.956	Kg	2.965	Kg	2.967	Kg	2.968	Kg
CHECK Chord	c	0.195	m	0.197	m	0.198	m	0.198	m
CHECK Weight variation	ΔW	0.033	Kg	0.009	Kg	0.002	Kg	0.001	Kg

LEGEND	
Input Data	
Iterations results	

Table 12 - Payload Data Input

PAYLOAD INPUT			
Name	**Symbol**	**Quantity**	**Unit**
Number of passengers	n	8	
Number of passengers for each row	N	2	
Passenger's length	a	0.031	m
Passenger's width	c	0.031	m
Passenger's height	l	0.09	m
Passenger's weight	M	113.4	g
Luggage length	a	0.019	m
Luggage width	c	0.025	m
Luggage height	l	0.038	m
Luggage weight	M	58	g

Table 13 – Aircraft Data Input

AIRCRAFT DATA INPUT			
Name	**Symbol**	**Quantity**	**Unit**
Wing Load	W/S	10	Kg/m^2
		98	N/m^2
Maximum landing lift coefficient	$CL_{max\_landing}$	1.8	
Maximum take-off lift coefficient	$CL_{max\_takeoff}$	1.5	
Take-off run	S_g	7.0	m
Wingspan	b	1.5	m
Aspect Ratio	AR	8.0	

Table 14 - Design Data

DESIGN			
Name	**Symbol**	**Quantity**	**Unit**
Stall speed - Landing	$V_{stall\_landing}$	3.0	m/s
Rate Thrust - Weight	T/W	0.0959	N/kg
Stall speed – Take-off	V_{stall_TO}	3.3	m/s
Rate Power-Weight	Π/W	5.257	W/N
	Π/W	51.57	W/Kg
Structural Weight + Payload Weight	$W_{struct+payload}$	2.764	Kg
Structural Weight	W_{struct}	1.393	Kg
Payload Weight	$W_{payload}$	1.371	Kg
Power Required	Π_n	142.6	W
Electronics Weight	W_{elect}	0.159	Kg
Total Starting Weight	W_{tot}	2.923	Kg

Table 15 - Payload Structure Information

PAYLOAD STRUCTURE INFORMATION			
Name	**Symbol**	**Quantity**	**Unit**
Number of rows	N	4	
Passenger and Luggage seat length	a1	0.060	m
Passenger and luggage seat width	c1	0.037	m
Passenger and luggage height	H	0.108	m
Total length of payload grid	A	0.240	m
Total width of payload grid	C	0.074	m
Final length of payload grid	A_{final}	0.264	m
Final width of payload grid	C_{final}	0.081	m
Front part length	r	0.204	m
Tail length	j	0.270	m
Aircraft Length	L	0.738	m
Payload Weight	$W_{payload}$	1371.2	g

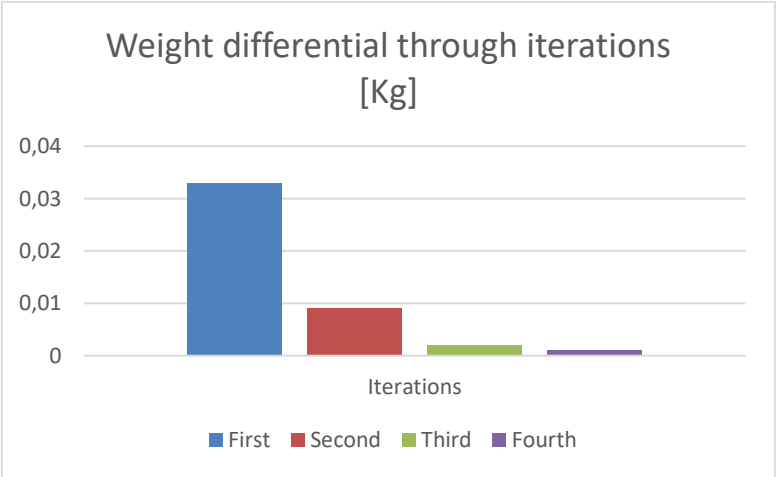

Figure 11 - Weight Differential through iterations

Table 16 - Weight Estimation

STATISTIC ESTIMATION			
STRUCTURAL WEIGHT ESTIMATION			
RATIOS ESTIMATION			
Name	**Symbol**	**Quantity**	**Unit**
Wing's ratio	W_{wing}/S_{wing}	1.8300	Kg/m^2
Fuselage's ratio	$W_{fus}/(D_{fus}\cdot L_{fus})$	8.3000	Kg/m^2
Horizontal tailplane's ratio	W_{H_tail}/S_{H_tail}	1.0600	Kg/m^2
Vertical tailplane's ratio	W_{V_tail}/S_{V_tail}	1.2500	Kg/m^2
WEIGHTS ESTIMATION			
Name	**Symbol**	**Quantity**	**Unit**
Wing surface	S_{wing}	0.2813	m^2
Fuselage diameter	D_{fus}	0.1296	m
Fuselage length	L_{fus}	0.7383	m
Horizontal tailplane surface	S_{H_tail}	0.0563	m^2
Vertical tailplane surface	S_{V_tail}	0.0197	m^2
Structural Weight	W_{struct}	1.393	Kg

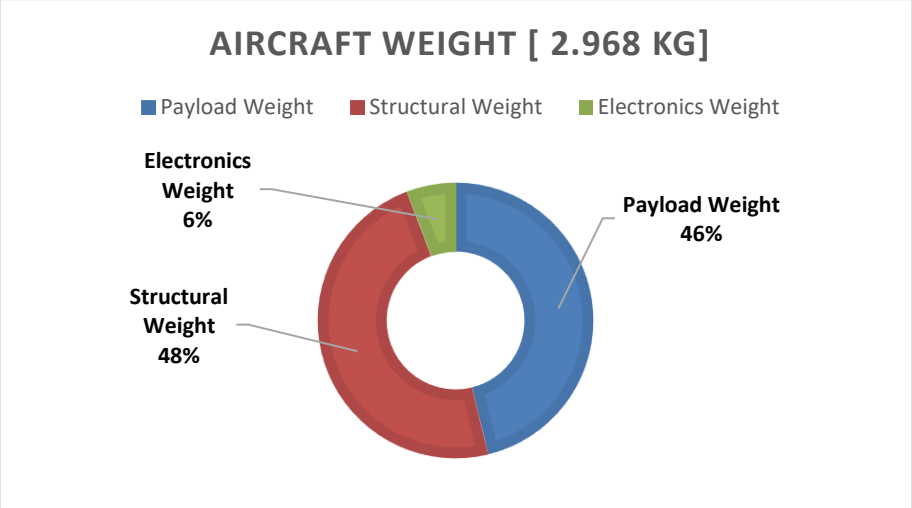

Figure 12 - Aircraft Weight

Considering the final values of weight regarding the electronics, we selected real components that very closely match the ones coming from our model. Regarding the single engine configuration, the propulsion will come from a “A20-22L EVO kv924” form *Hacker* with the paired ESC “X-12-Pro”. For the twin engine configuration, instead, the most suitable engine is “A20-30M EVO kv980”. The battery that will power the propulsive system will be a “20C-ECO-X 1450mAh 3S-slim” from *TopFuel*.

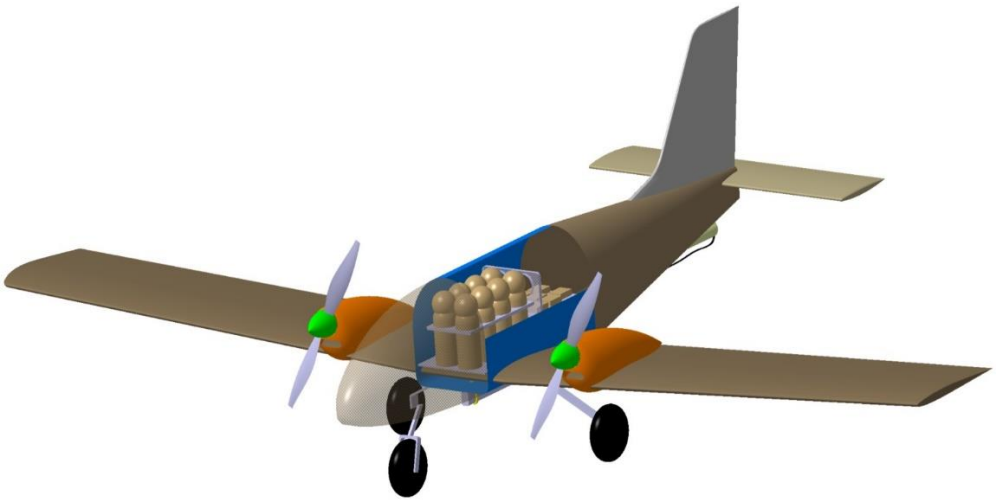

Figure 13 - First Aircraft Sketch

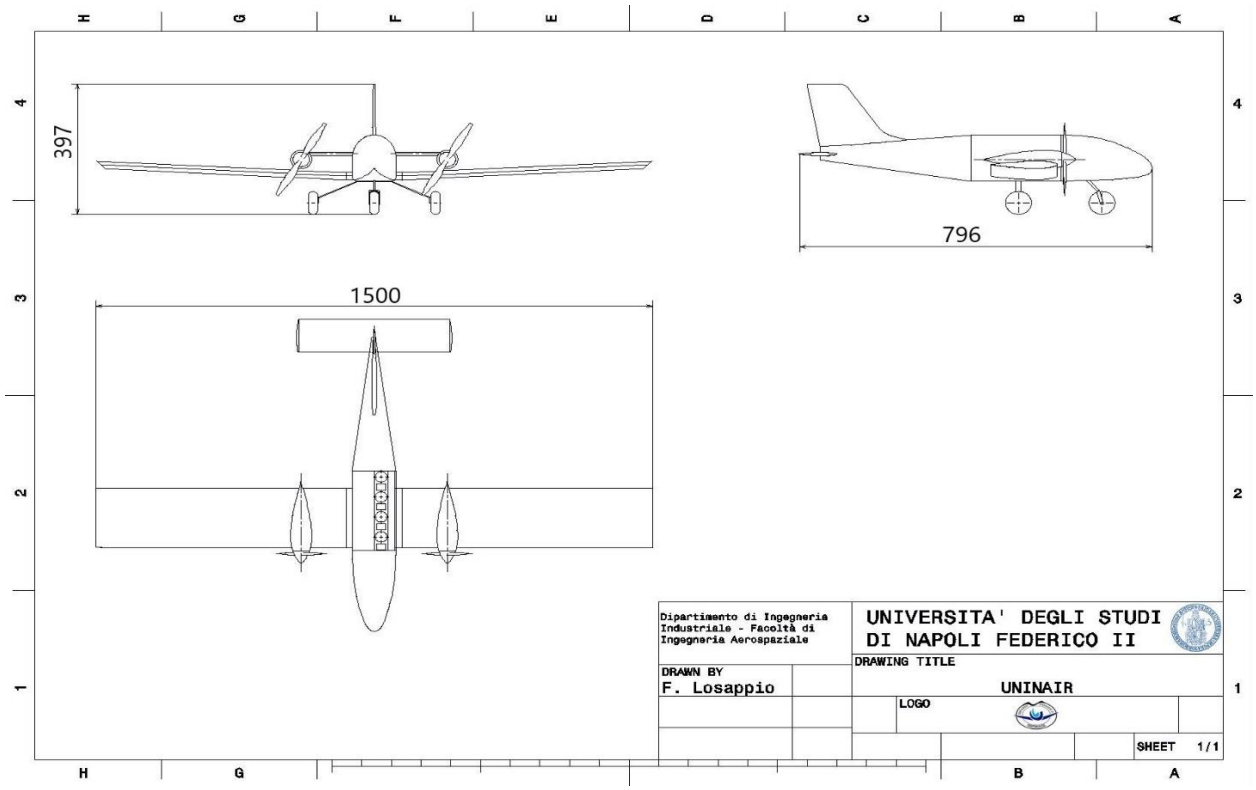

Figure 14 – Aircraft Three Views

Chapter 3
Lifting Surfaces Final Sizing

3. Introduction

In order to obtain the final sizing of the aircraft's lifting surfaces, it is advisable to carry out analysis of the aerodynamic characteristics, and the loads that arise on the lifting surfaces. To this end it has been made extensive use of the OpenVSP program, which first of all requires the creation of a first CAD model of the aircraft, and then moves on to the successive studies to be carried out. Below is an image of the model itself, created on the basis of the data determined in the preliminary sizing, while the missing ones were taken from similar models [1]-[2]:

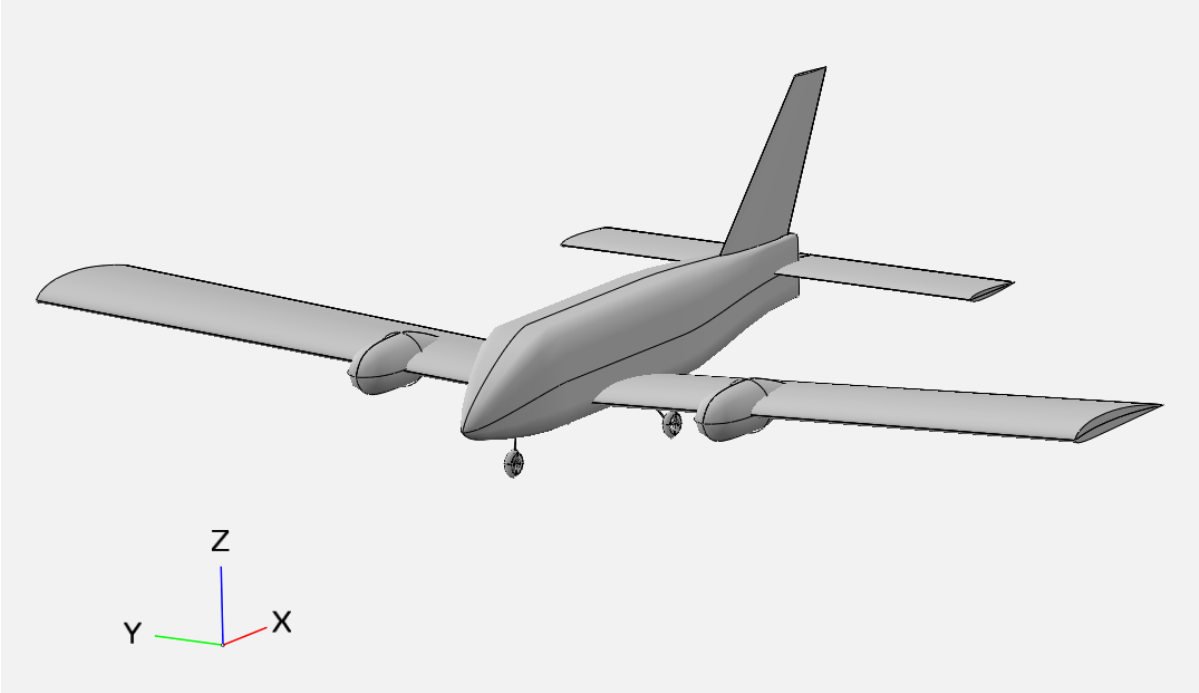

Figure 15 – OpenVSP Aircraft UNINAIR

It is also underlined that in the program itself 3 sets have been defined for the studies mentioned previously:

1) Wing
2) Wing + Horizontal Tail
3) Wing + Horizontal Tail + Vertical Tail

3.1 Wing

The entire geometry of the wing has not been modified from the one provided in the preliminary sizing, since it is satisfactory for the execution of the missions to be carried out, and also the chosen profile allows high aerodynamic performance.

Table 17 – Wing parameters

Parameter	Value
Airfoil	CLARK Y
M.A.C. $\bar{c}$	0.198 m
Span b	1.50 m
Area S	0.297 m^2
Aspect Ratio AR	7.55
Sweep Angle Λ	0°
Taper Ratio λ	1

Hereafter there are the main aerodynamic characteristics of the isolated wing, obtained through OpenVSP program, by varying the AoA input between 0 and 10 °, and by integrating a Reynolds number *Re* in the amount of 150.000. As output, the program returns an Excel spreadsheet with the coordinates of the characteristics of interest, which are then entered into a MATLAB code for a better representation. Moreover, always using this methodology, it is possible to recreate the polar of the isolated wing, based on the coordinates of the C_L and C_{Di} present in the Excel file. Later, the C_{D0} contribution (198 drag counts) is added, always obtained from OpenVSP program and in particular from the "Parasite Drag Analysis" tool [3], by choosing to consider an additional 5% growth caused by flaps and excrescences (e.g. screws).

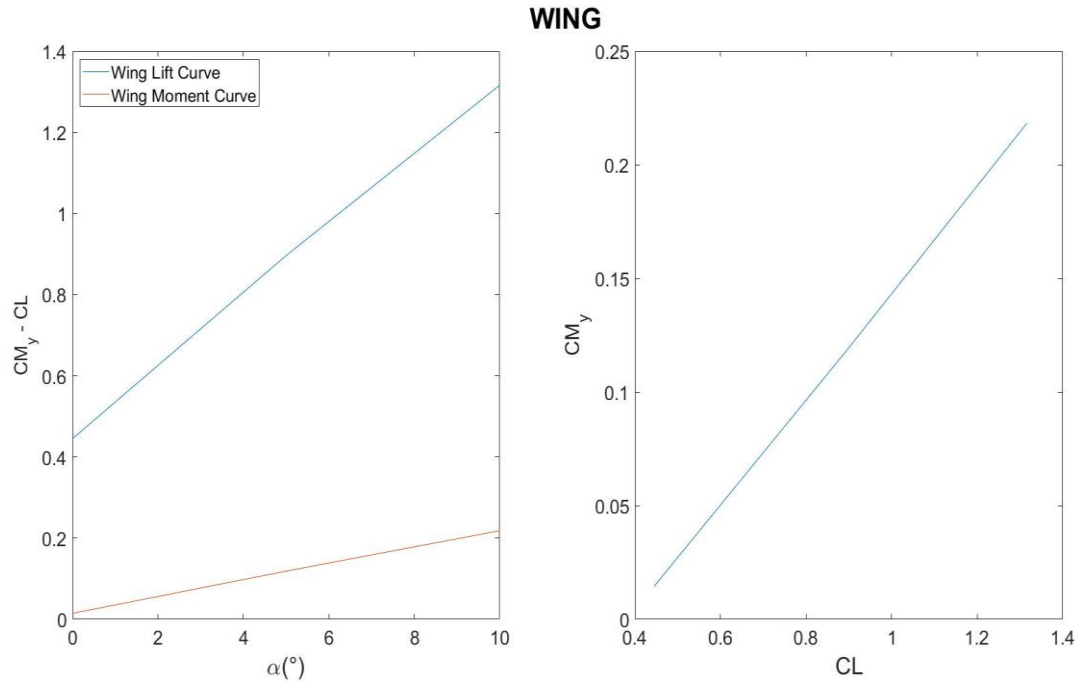

Figure 16 – Wing Set Aerodynamic Characteristics

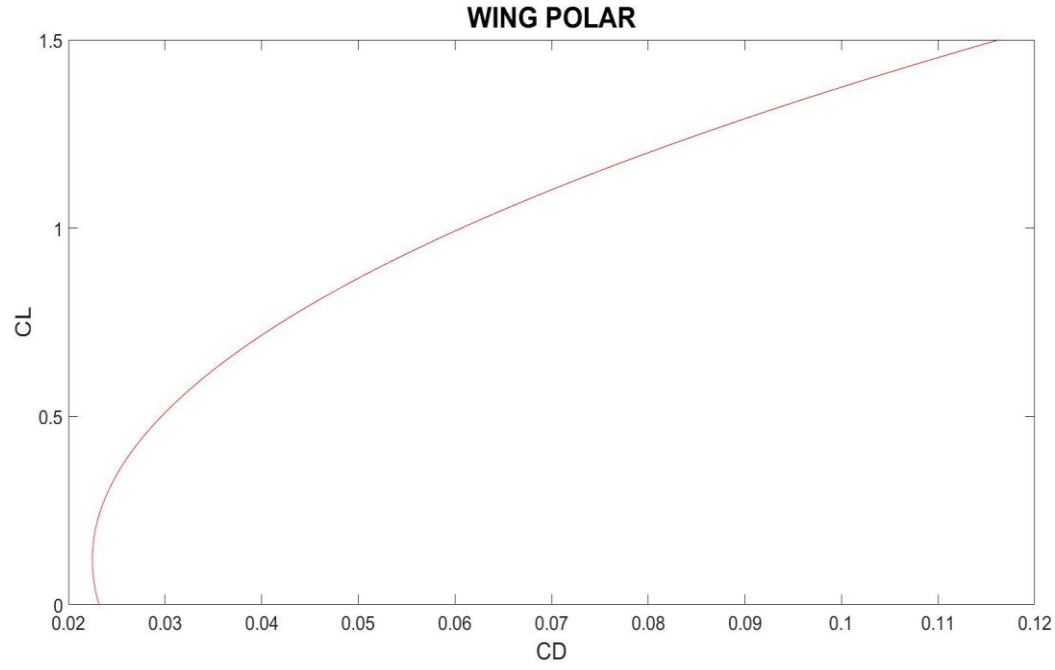

Figure 17 – Wing Polar

Finally, the analysis of the aerodynamic loads that insist on the isolated wing has been carried out. Figure 18 shows the diagrams of C_l distribution and aerodynamic loads $C_L \cdot c/c_{ref}$ as the AoA varies (red curves 0°, yellow 5°, green 10°):

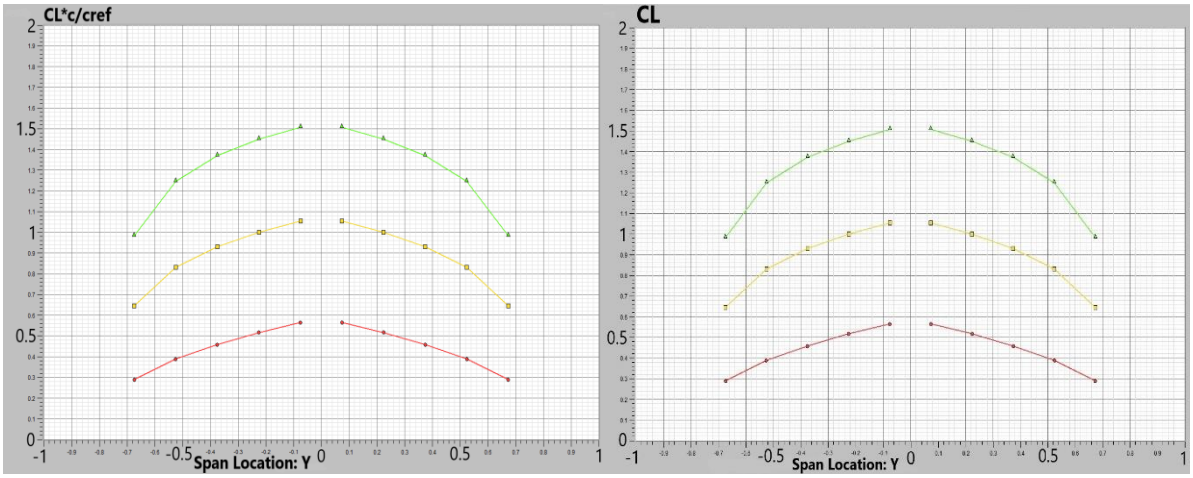

Figure 18 – Wing Set Loads

3.2 Wing + Horizontal Tail

As for the wing, the geometry of the horizontal tail has also remained the same as the geometry determined in the preliminary sizing:

Table 18 – Horizontal Tail parameters

Parameter	Value
Airfoil	NACA 0009
M.A.C. $\bar{c}_H$	0.100 m
Span b	0.59 m
Area S_H	0.059 m^2
Aspect Ratio AR	5.90
Sweep Angle Λ	0°
Taper Ratio λ	1

3.2.1 Downwash

In order to verify that the horizontal tail has been correctly sized, and then correctly positioned, it is necessary to verify that it doesn't result in the wake of the main wing, and therefore the study of the downwash phenomenon is fundamental. The latter is represented by the displacement of the air downwards due to the lifting action of the wing. Through this study, especially the "VSPAERO Analysis", carried out with OpenVSP [4], it was found that the

position of the horizontal tail, determined in the preliminary sizing, is such as to bring the tail itself in the wake of the wing. Moreover, the slope of the C_L-C_{My} curve is positive, which causes the horizontal empennage position to be changed by moving it further back (to increase the C_{My} arm, in order to enhance longitudinal stability) and/or increase its dimensions. It should be noted that the slope mentioned above is also known as the Safety Margin M.S., which must be negative to guarantee the stability of the aircraft. As a result, as seen in the images below, it has been only necessary to move the horizontal tail further back thus ensuring an M.S. negative, so that the tail itself does not lay in the wake of the wing. Note that the analysis was carried out at an AoA of 10 °.

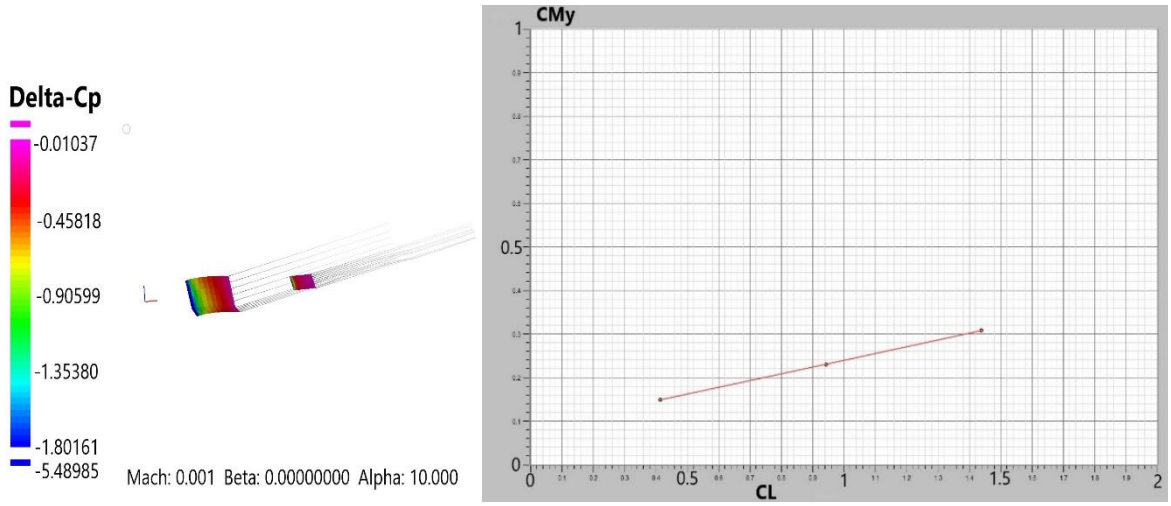

Figure 19 – Excessive Downwash and M.S. > 0

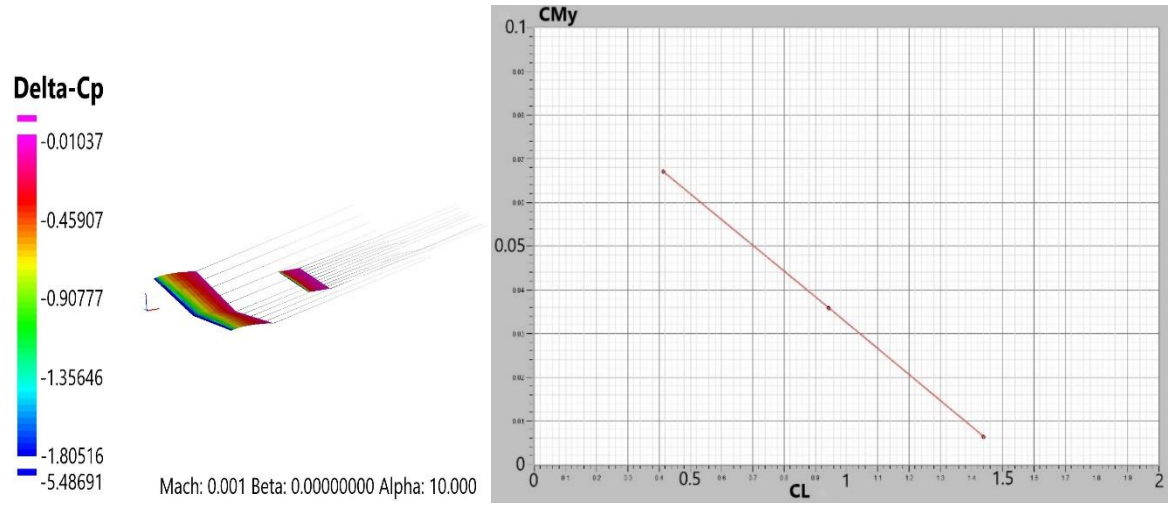

Figure 20 – Low Downwash and M.S. < 0

Finally, it is possible to numerically determine the value of the downwash through the relation $\frac{d\varepsilon}{d\alpha}|_{M=0} = \frac{2\,C_{L_{\alpha,W}}}{\pi\,AR_W e_W}$ with $C_{L_{\alpha,W}}$ and e_W determined by using the Polhamus formula, since the

latter is applicable in the hypothesis of $\Lambda_{le} < 32°$; $0.4 < \lambda \leq 1$; $3 \leq AR \leq 8$; $M < M_{cr}$ which are all satisfied with the wing geometry defined earlier. Therefore:

$$C_{L_{\alpha,W}} = \frac{2\,\pi\,AR_W}{2 + \sqrt{4 + \frac{{AR_W}^2(1-M^2)}{{k_p}^2}\left(1 + \frac{\tan\Lambda_{\frac{c}{2}}}{1-M^2}\right)}} = 5.05\ rad^{-1} = 0.088\ deg^{-1}$$

(note that this value could also be determined by calculating the slope of the curve C_L-α, shown above, still obtaining the same result), with

$$k_p = 1 + \frac{(8.2 - 2.3\,\Lambda_{le}) - AR\,(0.22 - 0.153\,\Lambda_{le})}{100} = 1.06$$

because $AR \geq 4$, and

$$e_W = \frac{2}{2 - AR + \sqrt{4 + AR^2\,(1 + \tan^2\Lambda_{tmax})}} = 0.88$$

From these formulas it has been determined $\frac{d\varepsilon}{d\alpha}|_{M=0} = 0.48$. As a final analysis, the downwash angles at the wing and at infinity downstream, at the test AoA (0°, 5°, 10°), can be determined through the relations $\varepsilon_{wing} = \frac{CL_W}{\pi\,AR_W}$ and $\varepsilon_\infty = \frac{2\,CL_W}{\pi\,AR_W}$. Downwash angles are reported in Table 19.

Table 19 – Downwash parameters

AoA (°)	$\in_{wing}$	$\in_\infty$
0	0.013	0.026
5	0.032	0.064
10	0.0505	0.1010

3.2.2 Set Analysis

Following the new sizing implemented, it is also possible to determine the Tail Volume Ratio $\bar{v}_H$ through the formula

$$\bar{v}_H = \frac{S_H}{S}\left(\bar{x}_{ac,H} - \bar{x}_{ac,W}\right) = 0.66$$

with

$$\bar{x}_{ac,H} = \frac{1}{\bar{c}}\left(\frac{\bar{c}_H}{4} + X_{le,\bar{c}_H}\right) = 3.56$$

and $\bar{x}_{ac,W} = 0.25$ with the different quantities highlighted in Figure 21 (note that $l_H = \bar{x}_{ac,H} - \bar{x}_{ac,W}$).

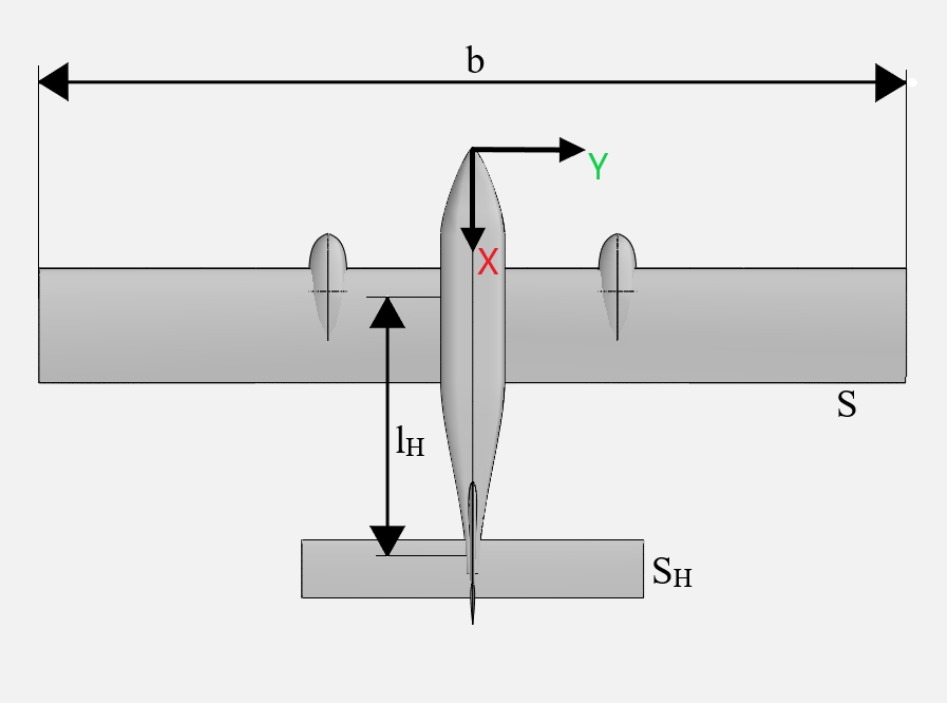

Figure 21 – Parameters for the definition of H.Tail Volume Ratio

To complete the sizing, it is necessary to determine the aerodynamic loads and characteristics, by considering the Wing + H.Tail set and by taking into account the diagrams previously highlighted, in the case of the isolated wing set:

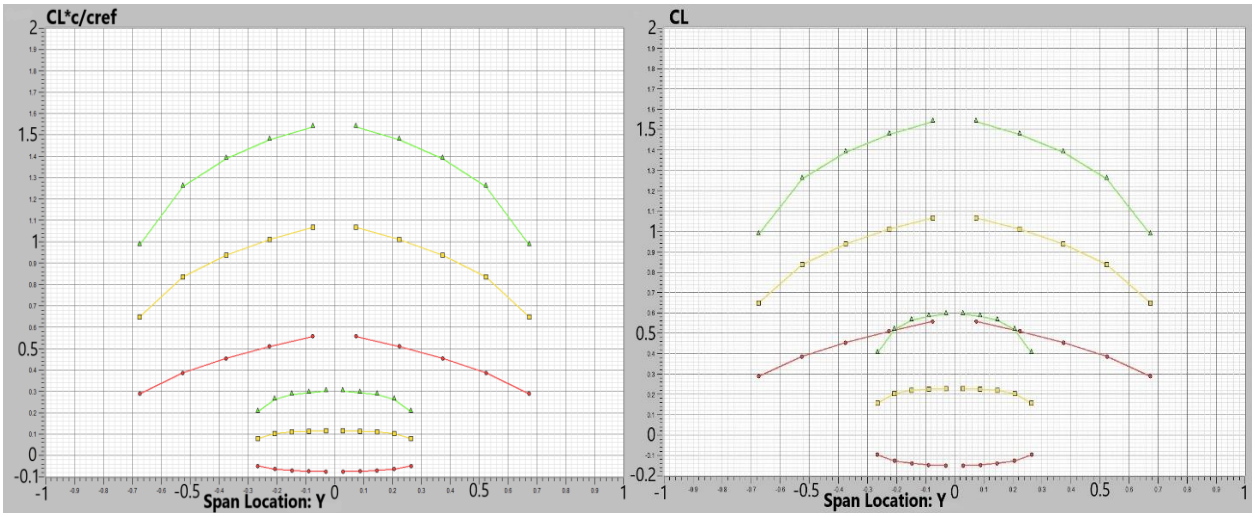

Figure 22 – Wing + H.Tail Set Loads

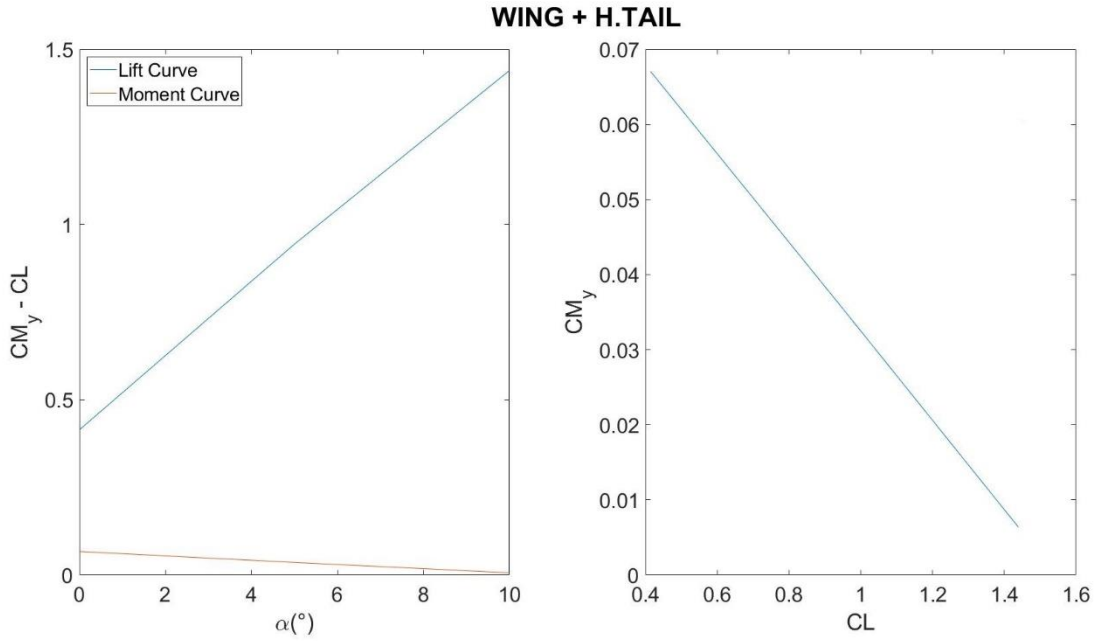

Figure 23 – Wing + H.Tail Set Aerodynamic Characteristics

The results obtained can also be considered valid by following the results of studies carried out on similar models [5] to [7].

The last Figure highlights that the stick fixed equilibrium ($C_M = 0$ and $\delta_e = 0$) is reached at an AoA over 10°. So that means that it is always necessary to trim for pitching in every cruise condition. Thus, to avoid this uncomfortable situation, it needs to be found the incidence angle i_H which guarantees the equilibrium. It is possible by manipulating the equilibrium (in rotation) formula

$$C_M = C_{M_0} + C_{M_\alpha}\alpha_B + C_{M_{i_H}} i_H = 0$$

where C_{M_0} is the Pitching Moment Coefficent at zero lift and it can be deduced from Figure 23 (2.87 rad^{-1}); C_{M_α} is the Pitching Curve Slope, also deducible from Figure 23 (-0.01 deg^{-1}); α_B is the cruise AoA (2°); $C_{M_{i_H}}$ represents the Pitch Control Power and it is determined by using the relation

$$C_{M_{i_H}} = -\eta_H \, \bar{v}_H \, C_{L_{\alpha,H}} = -0.8\, rad^{-1}$$

where η_H is the dynamic pressure's degradation factor and it can be assumed as the 90% of q_∞; $C_{L_{\alpha,H}}$ is the Lift Curve Slope of the horizontal tail (0.024 deg^{-1} = 1.35 rad^{-1}).

At the end it results $i_H = 0.052\, rad = 3\, deg$ (during the rotation, the pivot is located at the 25% of the chord).

Hence the diagrams in the last Figure can be updated as showed in Figure 24:

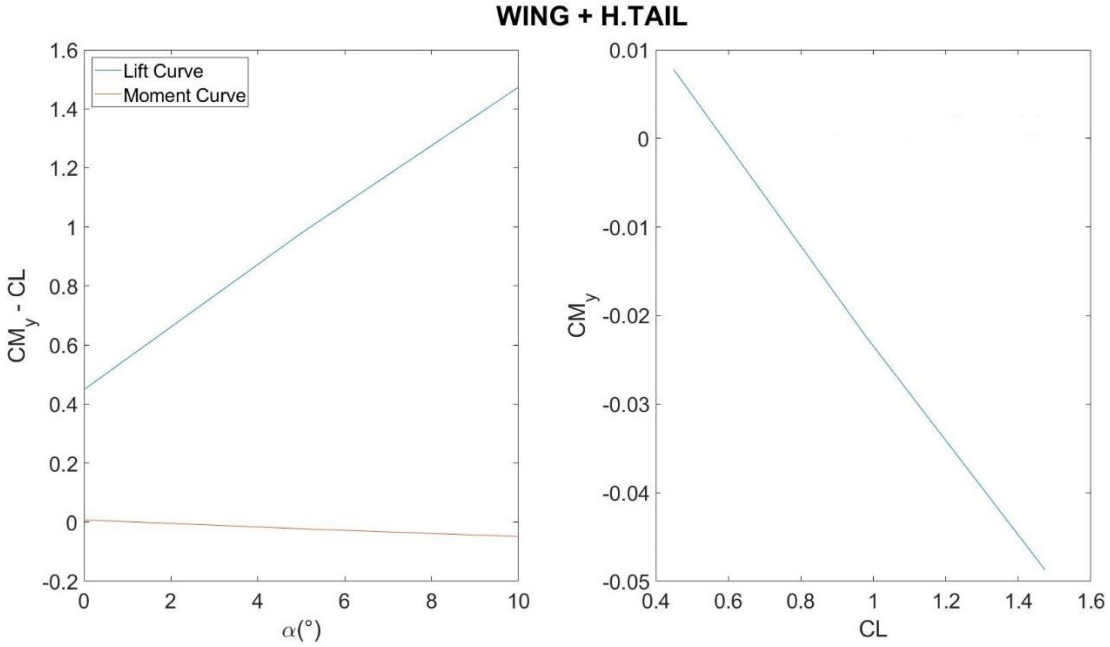

Figure 24 - Wing + H.Tail Set with Tail incidence

Now, for every C_L, there will be either negative C_{My} or positive C_{My}. In the previous condition, for every C_L, there were only positive ones.

3.2.3 Fuselage Contribution

To certify that the value of $\bar{x}_{ac,W}$ obtained from the sizing is plausible, it must be verified that, with the addition of the fuselage, the aerodynamic center moves forward and therefore must be $\bar{x}_{ac,WB} < \bar{x}_{ac,W}$. To determine $\bar{x}_{ac,WB}$ it has to refer to the relation

$$\bar{x}_{ac,WB} = \bar{x}_{ac,W} - \frac{C_{M_{\alpha,B}}}{C_{L_{\alpha,W}}}$$

in which only $C_{M_{\alpha,B}}$ is unknown, but it can be obtained through the "Strip Method" [8]:

$$C_{M_{\alpha,B}} = \frac{C_{L_{\alpha,W}}}{2.87\ S\ \bar{c}} \sum_{k=1}^{3} {w_k}^2\ \Delta x_k\ \frac{d\bar{\varepsilon}}{d\alpha}$$

As a result, the fuselage must be divided into six sections as shown in the Figure 25.

Besides, Table 20 contains all the coefficients necessary to perform the summation to obtain the $C_{M_{\alpha,B}}$. Note that yellow points represent the centroids of each section k, Δx_k represents the extension of each section, w_k is the local width of each section and $\left(\frac{d\varepsilon}{d\alpha}\right)_k$ is the upwash (from

the nose to the LE)/downwash (from the TE to the fuselage's tail) contribute to which each section is subjected.

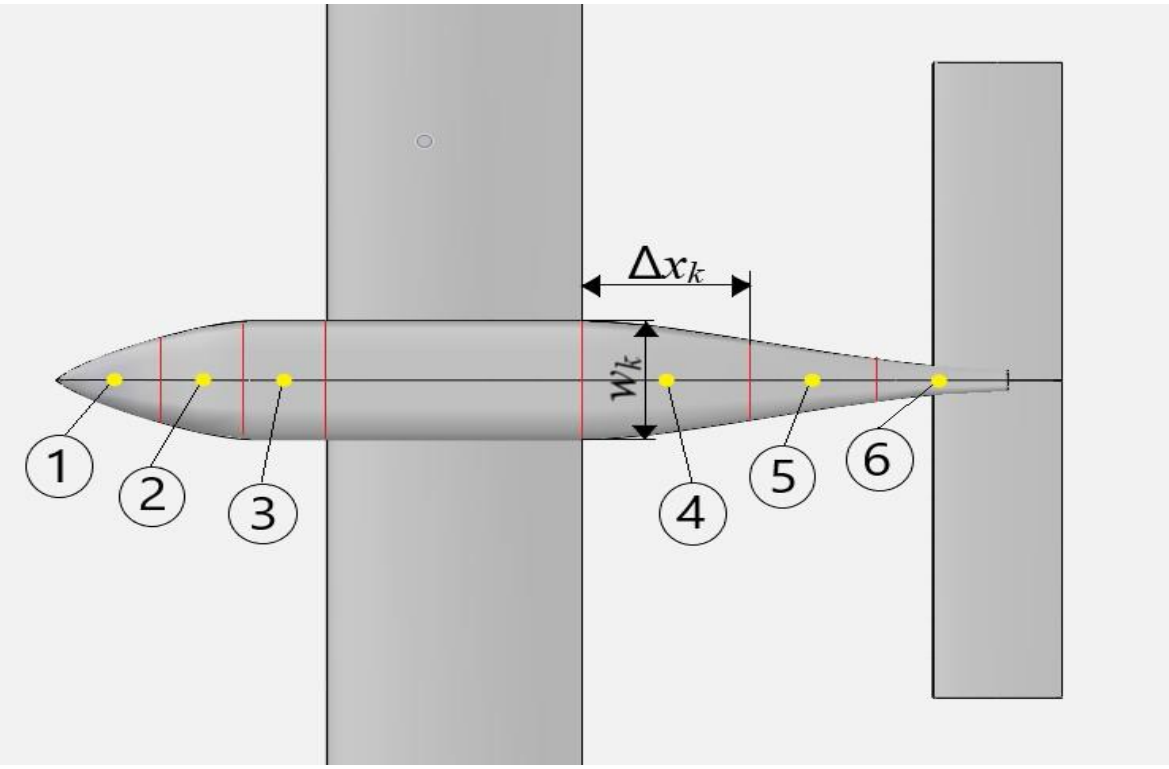

Figure 25 – Fuselage sections

Table 20 – Multhopp's coefficients

Section k	Δx_k	w_k	$\left(\frac{d\varepsilon}{d\alpha}\right)_k$	$w_k^2\,\Delta x_k$	$w_k^2\,\Delta x_k\left(\frac{d\varepsilon}{d\alpha}\right)_k$
1	0.07	0.08	0.125	$4.5 \cdot 10^{-4}$	$6 \cdot 10^{-5}$
2	0.06	0.11	1.9	$7.3 \cdot 10^{-4}$	$1.4 \cdot 10^{-3}$
3	0.08	0.11	2.5	$9.7 \cdot 10^{-4}$	$2.4 \cdot 10^{-3}$
4	0.12	0.11	0.05	$1.45 \cdot 10^{-3}$	$7.3 \cdot 10^{-5}$
5	0.10	0.09	0.25	$8.1 \cdot 10^{-4}$	$2 \cdot 10^{-4}$
6	0.11	0.07	0.51	$5.4 \cdot 10^{-4}$	$3 \cdot 10^{-4}$

So, in the end $C_{M_{\alpha,B}} = 0.13\,rad^{-1} \rightarrow \bar{x}_{ac,WB} = 0.224 \rightarrow \Delta\bar{x}_{ac} = 0.026$. As a result, the x_{ac} has been moved forward as the fuselage was added. It is appropriate to point out that this result is plausible, if we were analysing aircraft and not just models [9]-[10].

3.2.4 Longitudinal Stability

The previous studies show that this set has a $\bar{x}_G = 0.3$, the neutral point $\bar{x}_N$ can be determined by the formula:

$$C_{M_\alpha} = C_{L_\alpha} (\bar{x}_G - \bar{x}_N)$$

with

$$C_{L_\alpha} = C_{L_{\alpha,W}} + \eta_H \frac{S_H}{S} C_{L_{\alpha,H}} \left(1 - \frac{d\varepsilon}{d\alpha}\right) = 5.2\, rad^{-1} = 0.1\, deg^{-1}$$

Hence, it results $\bar{x}_N = 0.4$. Also note that $M.S. = \frac{C_{M_\alpha}}{C_{L_\alpha}} = \bar{x}_G - \bar{x}_N = -0.10$. Note that this value could also be determined by using the formula

$$\bar{x}_N = \frac{\bar{x}_{ac,WB} + \frac{C_{L_{\alpha,H}}}{C_{L_{\alpha,W}}} \eta_H \bar{x}_{ac,H} \frac{S_H}{S} \left(1 - \frac{d\varepsilon}{d\alpha}\right)}{1 + \frac{C_{L_{\alpha,H}}}{C_{L_{\alpha,W}}} \eta_H \frac{S_H}{S} \left(1 - \frac{d\varepsilon}{d\alpha}\right)}$$

From the analysis carried out by considering the Wing set and the Wing + H.Tail set, it is possible to deduce some parameters, already calculated, which determine the longitudinal stability, and they are reported in Table 21:

Table 21 – Longitudinal stability

Parameter (at $\bar{x}_G = 0.3$)	Symbol	Value	Unit
Neutral point	$\bar{x}_N$	0.40	-
Airplane longitudinal stability (*M.S.*)	$\frac{C_{M_\alpha}}{C_{L_\alpha}}$	-0.1	-
Airplane pitching curve slope (total)	C_{M_α}	-0.01	deg^{-1}
Airplane lift curve slope (total)	C_{L_α}	0.1	deg^{-1}
Aerodynamic center shift due to fuselage	$\Delta\bar{x}_{ac}$	0.026	-
Wing aerodynamic center	$\bar{x}_{ac,W}$	0.25	-

3.3 Wing + Empennage

The last lifting surface to be added to those previously described is the vertical tail, whose geometry, again, has not been changed. Unlike the main wing and the horizontal tail, which

are both rectangular, the vertical empennage is a sweep wing with the following characteristics:

Table 22 – Vertical Tail parameters

Parameter	Value
Airfoil	S9026
M.A.C. $\bar{c}_V$	0.110 m
Span b	0.195 m
Area S_V	0.021 m^2
Aspect Ratio AR	1.77
Sweep Angle Λ	40°
Taper Ratio λ	0.47

Since it is a sweep wing $\bar{c}_V = \frac{2}{3} c_r \frac{1+\lambda+\lambda^2}{1+\lambda}$ with $c_r = 0.15$.

3.3.1 Set Analysis

As previously done for the horizontal tail, it is also possible to calculate the Tail Volume Ratio $\bar{v}_V$ of the vertical tail by using the relation $\bar{v}_V = \frac{S_V}{S}\frac{l_v}{b} = 0.018$ with $l_v = X_{le,r,V} + \frac{\bar{c}_v}{4} - X_G + X_{le,\bar{c}_V} = 0.375$. The useful elements for the calculation are shown in the following image:

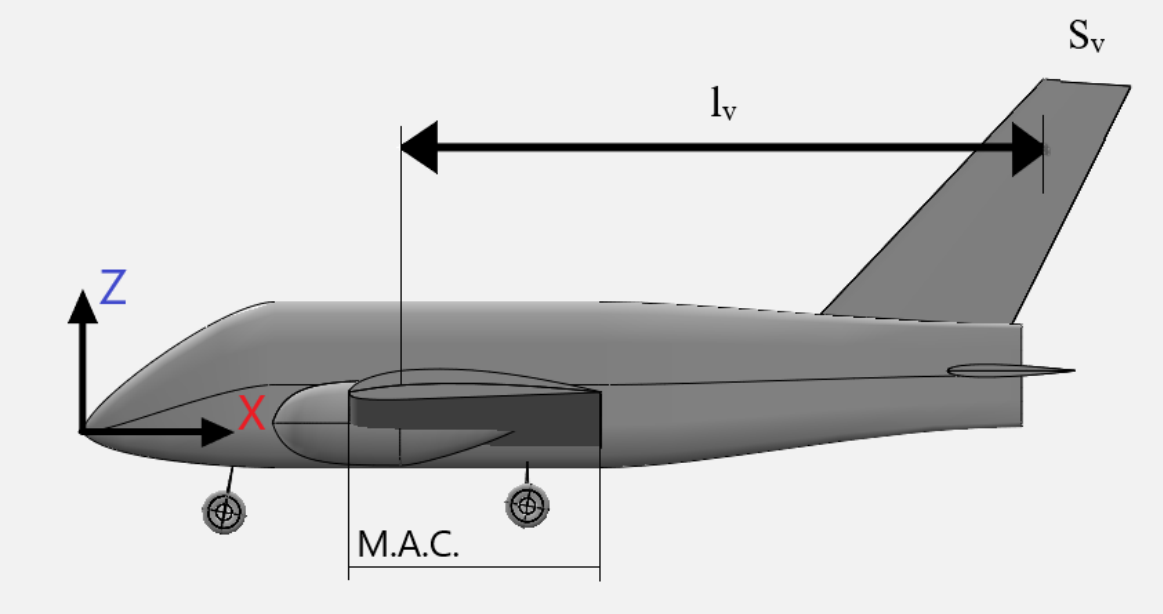

Figure 26 – Parameters for the definition of V.Tail Ratio

Below are the aerodynamic characteristics analysed in the previous sets, but in this case it is also taken into account the vertical empennage. Since the vertical tail does not affect the longitudinal aerodynamic characteristics of the aircraft model, it is more useful to investigate its contribution to yaw and roll.

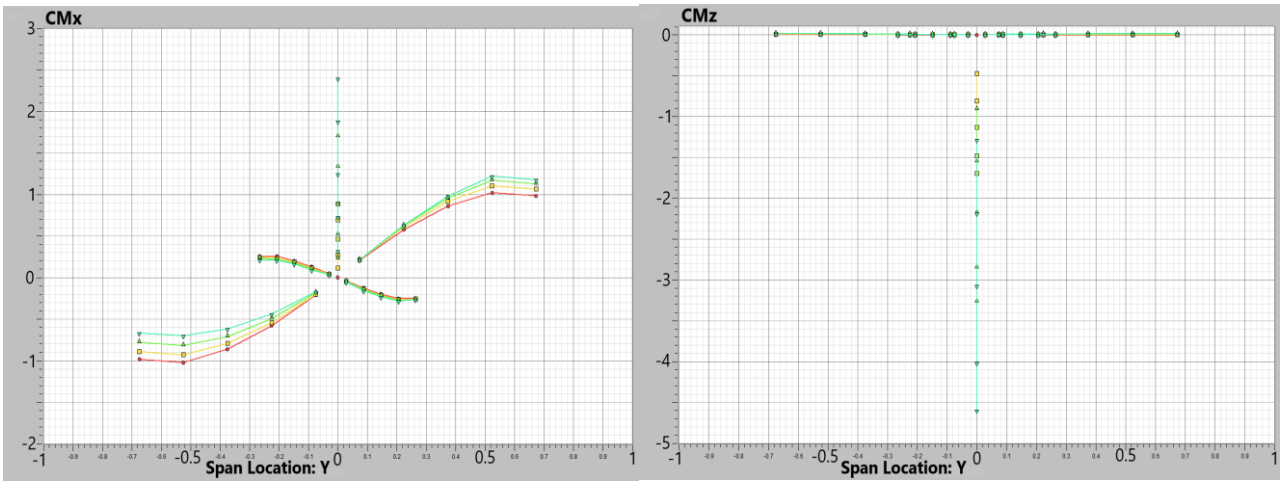

Figure 27 – Wing + Empennages Set Aerodynamic Loads

3.3.2 Directional Stability

The addition of the vertical tail allows to study the directional stability with the presence of crosswind, which induces a drift angle β (positive if wind comes from the left considering a front view as in Figure 28). It is therefore possible to carry out analysis of $C_{N\beta}$, since the latter can be determined from the relation $C_{N_\beta} = C_{N_\beta}|_V + C_{N_\beta}|_F$, with the addends respectively representing the contributions of the vertical empennage and the fuselage.

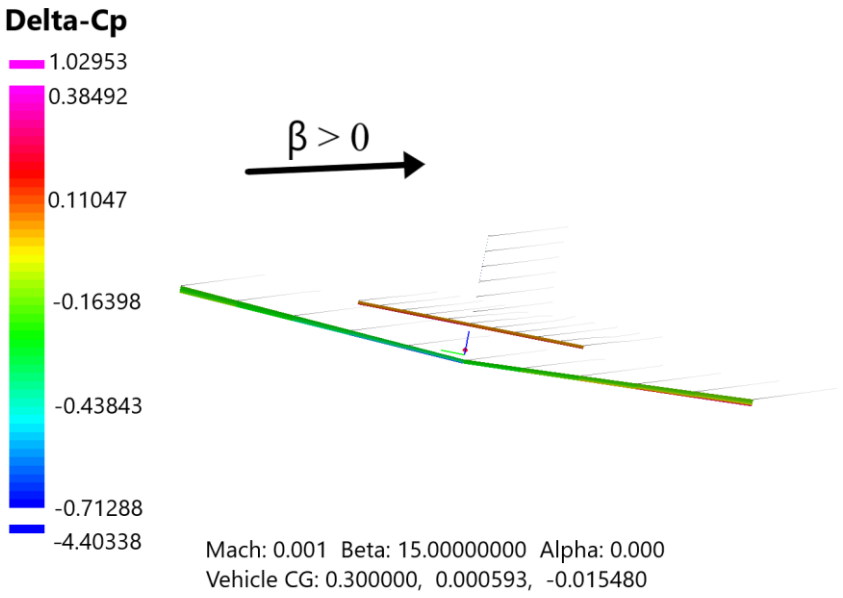

Figure 28 – Convention for β

To determine the contribution of the vertical tail, the "VSPAERO Analysis" is used, inserting as input a variable drift angle (0 °, 5 °, 10 °, 15 °) and a *Re* equal to 150.000. It should be noted, by the figure below, that $C_{N_\beta}|_V$ does not change if we consider the set composed only either by the vertical tail or the set wing + tail. The figure also shows the $C_{L\beta}$ curve (*L* intended as rolling moment):

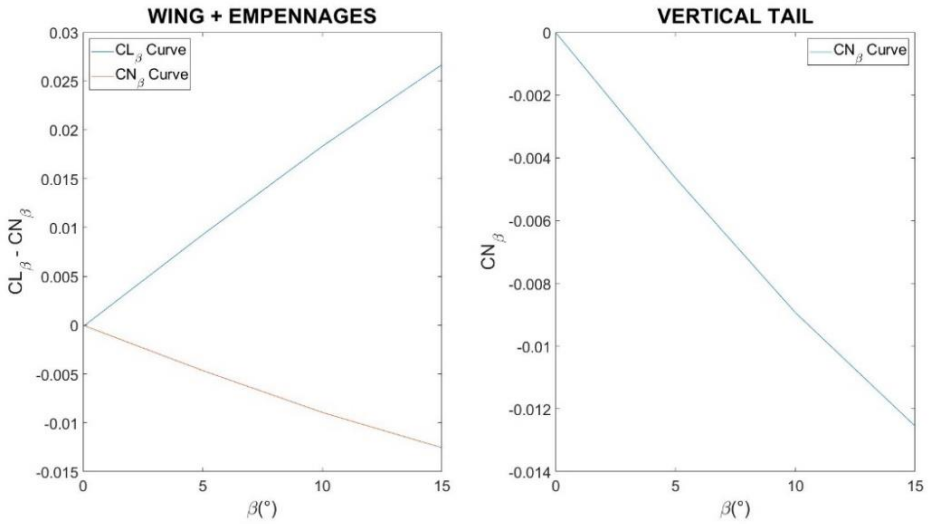

Figure 29 – $C_{N\beta}$ and $C_{L\beta}$ curves

From Figure 29, it can be deduced, by calculating the slope of the red curve, that $C_{N_\beta}|_V = -8 \cdot 10^{-4}\ deg^{-1}$, and in addition the slope of the blue curve is $C_{L_\beta}|_V = 1.7 \cdot 10^{-3}\ deg^{-1}$. The contribution due to the fuselage can be obtained from the formula $C_{N_\beta}|_F = 57.3\ K_N K_{Re,\beta}\ \frac{S_{Bs}\ l_B}{S\ b}$ assuming that the area of the S_{Bs} side view is equal to 70% of the area of the rectangle surrounding it, and also the coefficients $K_{Re,\beta}$ and K_N are deductible from the following diagrams:

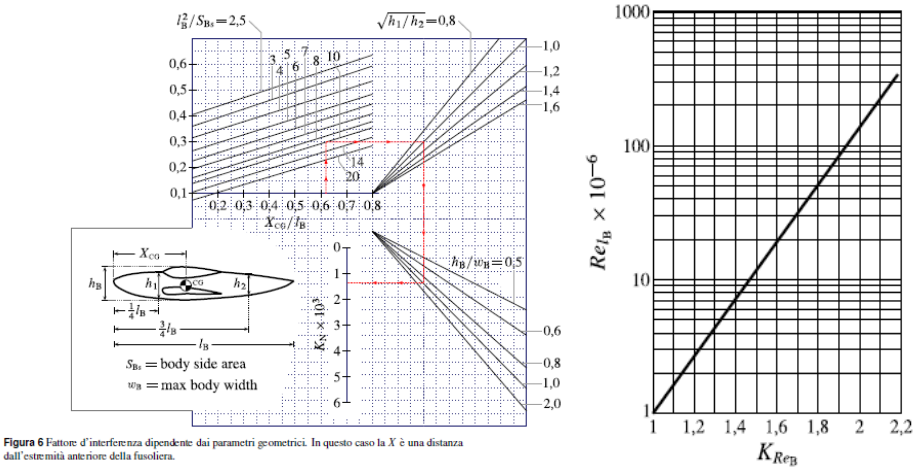

Figura 6 Fattore d'interferenza dipendente dai parametri geometrici. In questo caso la X è una distanza dall'estremità anteriore della fusoliera.

Figure 30 – $K_{(Re,\beta)}$ and K_N charts

So it turned out $C_{N_\beta}|_F = 0.02\, rad^{-1} = 3.5 \cdot 10^{-4}\, deg^{-1} \rightarrow C_{N_\beta} = -4.5 \cdot 10^{-4}\, deg^{-1}$. In summary, the fundamental parameters for directional stability are contained in the following table:

Table 23 – Directional stability

Parameter (at $\bar{x}_G = 0.3$)	Symbol	Value	Unit
Fuselage contribution	$C_{N_\beta}\|_F$	$3.5 \cdot 10^{-4}$	deg^{-1}
Vertical tail contribution	$C_{N_\beta}\|_V$	$-8 \cdot 10^{-4}$	deg^{-1}
Airplane directional stability	C_{N_β}	$-4.5 \cdot 10^{-4}$	deg^{-1}

It is also noted that these results are verified, by comparing them with those obtained from aircraft with similar characteristics and geometries [11]-[12].

3.4 Aircraft Polar

Following the final sizing of the lifting surfaces, it is finally possible to obtain the polar of the whole aircraft, by adding the fuselage, the landing gear and the engines. The methodology for reconstructing the polar is the same applied to obtain that of the isolated wing. In this case, however, an increase of 10% is considered, given the entire model covered by this study. The following is the screenshot of the "Parasite Drag Analysis" tool, which also contains the contributions of wet surfaces of each component as well as each of their contributions from the point of view of drag:

Component	S_wet (m²)	Group	FF Equation	FF	L_ref (m)	t/c or l/d	Re (1e5)	% Lam	C_f (1e-3)	f (m²)	C_D	% Total
(+) Wing	0.55	SELF	Hoerner	1.25	0.198	0.117	2.03	0.0	6.13	0.0050	0.01692	32.50
(+) WheelL	0.00	SELF	Hoerner	63.04	0.010	1.000	0.10	0.0	12.63	0.0019	0.00625	12.01
(+) WheelR	0.00	SELF	Hoerner	63.04	0.010	1.000	0.10	0.0	12.63	0.0019	0.00625	12.01
(+) WheelAnt	0.00	SELF	Hoerner	63.04	0.010	1.000	0.10	0.0	12.63	0.0019	0.00624	11.99
(+) Fuselage	0.25	SELF	Hoerner Stre	1.15	0.739	5.675	7.59	0.0	4.71	0.0013	0.00449	8.63
(+) H.Tail	0.12	SELF	Hoerner	1.21	0.100	0.100	1.03	0.0	7.11	0.0011	0.00354	6.81
(+) V.Tail	0.05	SELF	Hoerner	1.21	0.115	0.100	1.18	0.0	6.90	0.0004	0.00132	2.53
(+) Engine L.	0.02	SELF	Hoerner Stre	1.49	0.200	3.162	2.05	0.0	6.12	0.0003	0.00114	2.20
Engine R._0	0.02	SELF	Hoerner Stre	1.49	0.200	3.162	2.05	0.0	6.12	0.0003	0.00114	2.20
(+) GearR	0.00	SELF	Hoerner Stre	1.01	0.050	31.620	0.51	0.0	8.35	0.0000	0.00001	0.01
(+) GearL	0.00	SELF	Hoerner Stre	1.01	0.050	31.620	0.51	0.0	8.35	0.0000	0.00001	0.01
(+) GearAnt	0.00	SELF	Hoerner Stre	1.01	0.050	31.620	0.51	0.0	8.35	0.0000	0.00000	0.01

Excrescence	Type	Input			
EXCRES_0	% of CD_Geom	10.00000	0.0014	0.00473	9.09

	f (m²)	C_D	% Total
Geom:	0.0141	0.04732	90.9
Excres:	0.0014	0.00473	9.1
Total:	0.0155	0.05205	100.0

Figure 31 – C_{D0} calculation

Furthermore, the MATLAB script is attached, through which the polar of the aircraft is reconstructed:

Polar_Curve.m

```
clear all; close all; clc;

CL = linspace(0,1.5,250);
ew = 0.88; % Fattore di Oswald
ARw = 8; % Aspect Ratio
CD0 = 0.052; % Coefficiente di Resistenza a portanza nulla
k = 1/(pi*ARw*ew);

CD = CD0 + k*(CL).^2;

plot(CD,CL,'b.'); axis([0 0.3 0 2]);
xlabel('CD'); ylabel('CL'); title('Polar Curve');

```

Figure 32 – Polar script

Finally, the polar of the aircraft is reported by comparing the polar returned by the "VSPAERO Analysis" and that determined by the MATLAB script. The former takes into account only the C_D and C_{Di}, the latter, on the other hand, is reconstructed by determining the parabola that passes through the 3 pairs of points (C_L, C_{Di}) returned by the OpenVSP Excel file by using the "polyfit" command. Subsequently, the C_{D0} contribution (520 drag counts) deriving from the "Parasite Drag Analysis" tool is added to the known term of the parabola itself, and finally everything is reported on a graph with the "polyval" command:

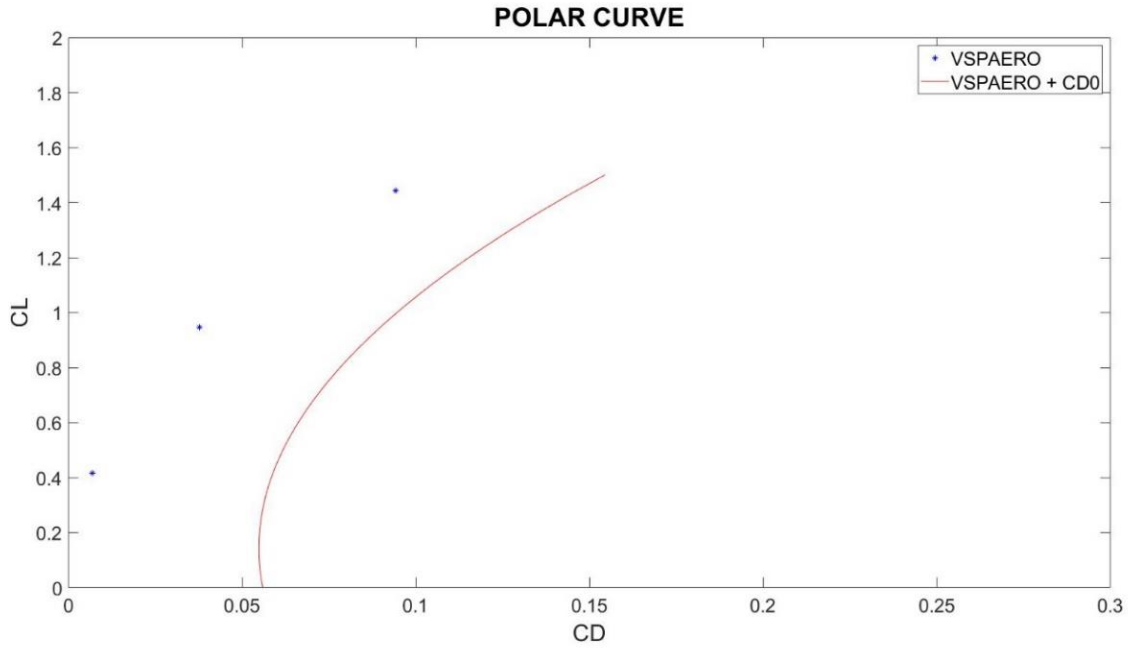

Figure 33 – Aircraft Polar

Bibliography

[1] GUDMUDSSON S. (2014) General Aviation Aircraft Design: Applied Method and Procedures, Elsevier, ISBN 978-0-12-397308-5

[2] GALE F. (1996) Dimensionamento Pratico di Aerostrutture, NASAR

[3] http://openvsp.org/wiki/doku.php?id=parasitedrag

[4] http://openvsp.org/wiki/doku.php?id=vspaerotutorial

[5] OBERT E. (2009) Aerodynamic Design of Transport Aircraft, Delft University of Technology, Delft, ISBN 978-1-58603-970-7

[6] RAYMER D. P. (1992) Aircraft Design: A Conceptual Approach, 2nd ed., AIAA, Washington, ISBN 0-930403-51-7

[7] TORENBEEK E. (1976) Synthesis of Subsonic Airplane Design, Delft University Press, Delft, ISBN 90-298-2505-7

[8] Agostino De Marco, Domenico P. Coiro, Fabrizio Nicolosi (2017) Elementi di Meccanica del Volo

[9] Jacobs E. and Ward, K. (1935) Interference of wing and fuselage from tests of 209 combinations in the NACA variable-density test tunnel. NACA Technical Report No. 540

[10] Maughmer,M., Hallmann,D., Ruszkowski, R., Chappel, G. and Waitz, I (1989) Experimental investigations of wing-fuselage integration geometries, AIAA Journal of Aircraft, 26(8)

[11] PERKINS C. D. and HAGE R. E. (1949) Airplane Performance Stability and Control, Wiley, New York, ISBN 0-471-68046-X

[12] FINCK R. D. (1978) USAF Stability and Control DATCOM, AFWAL-TR-83-3048, Wright-Patterson Air Force Base, McDonnell Douglas Corporation, Ohio

Un sentito ringraziamento a tutte le persone che mi hanno permesso di arrivare fin qui e di portare a termine questo lavoro di tesi.

Ringrazio il mio relatore Danilo Ciliberti, per la disponibilità, per le conoscenze trasmesse e per i suoi indispensabili consigli.

Ringrazio il mio correlatore Fabrizio Nicolosi per avermi dato l'opportunità di redigere questo elaborato.

Ringrazio di cuore i miei genitori e i miei nonni, perché mi hanno sempre sostenuto e mi hanno permesso di coltivare la mia passione più grande.